Atomic and Molecular Clusters in Membrane Mimetic Chemistry

JANOS H. FENDLER

Department of Chemistry, Syracuse University, Syracuse, New York 13244-1200

Received February 4, 1987 (Revised Manuscript Received April 20, 1987)

Contents

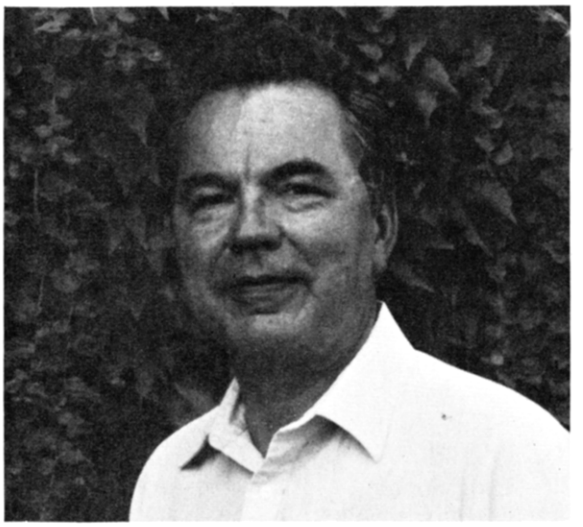

Janos H. Fendler, born in 1937 in Hungary, is now a naturalized U.S. citizen. He received his B.Sc., Ph.D., and D.Sc. degrees in England. After a postdoctoral fellowship at the University of California at Santa Barbara, Fendler spent 4 years (1966–1970) at the Mellon Institute in Pittsburgh. He rose through the academic ranks at Texas A&M University (1970–1981). Subsequent to an interlude at Clarkson University (1982–1985), Fendler joined Syracuse University where he is now Distinguished Professor of Chemistry and Director of the recently formed Center for Membrane Engineering and Science. Janos H. Fendler coined the phrase "membrane mimetic chemistry" to describe an approach that has served to unify seemingly disparate subjects, broad ranges of methodologies, and different terminologies. He has utilized surfactant assemblies—aqueous and reversed micelles, vesicles and polymerized vesicles, and bilayer lipid membranes (BLMs)—for molecular organization and compartmentalization. This, in turn, has led to catalyst, semiconductor, and magnetic particle stabilizations and utilizations, as well as to reactivity control. His researches have been reported in more than 170 publications and summarized in 30 review articles and 2 books. The research achievements of Janos H. Fendler have been recognized by several awards, including the Langmuir Distinguished Lecturer Award in 1979 and the ACS National Award in Colloid or Surface Chemistry in 1983, and by frequent invitations to be a plenary lecturer at national and international meetings. He has served on the editorial boards of several ACS journals.

I. Scope

Attention in this review is focused on novel chemistries developed by the use of surfactant assembly incorporated atomic and molecular clusters. Aqueous micelles, reversed micelles, microemulsions, vesicles, polymerized vesicles, monolayers, deposited organized multilayers [Langmuir–Blodgett (LB) films], and bilayer (black) lipid membranes (BLMs) are the host surfactant assemblies for the clustered particles. Controllable sized crystalline and amorphous materials, metals, and semiconductors are the clustered particles considered here.

There are several functions of the organized assemblies. They provide size, geometrical control, and stabilization for the clusters. However, organized surfactant assemblies are not only passive hosts. Hydrophobic and electrostatic interactions profoundly influence the chemical properties of the clusters. This, in turn, leads to interesting and often novel chemistries.

Inspiration for the investigations of controlled-size particles in organized assemblies can be sought from the biological membranes. The term "membrane mimetic chemistry" has been coined to describe relatively simple systems that mimic aspects of biomembranes. The philosophy of this approach is briefly described (section II) along with the different systems used in mimicking biomembranes (section III). The recently recognized importance of cluster formation in biology, biomineralization, is briefly surveyed in section IV. Section V summarizes the quantum size effects of ultramsall colloidal clusters.

Subsequent to introducing these diverse areas, the rationale for the membrane mimetic approach in the utilization of clusters is delineated in section VI. This approach is considered to bridge the biology of mineralization and the physics of quantum size effects in ultrasmall particles.

Sections VII–X critically discuss the available results on precipitation and crystallization, catalyst, semiconductor and magnetic particle formation, stabilization, and utilization in the different membrane mimetic systems. An attempt will be made to cover the reported results exhaustively.

Perspectives and prospects of the subjects reviewed are speculated on in the final section.

II. Philosophy of Membrane Mimetic Chemistry

Biological membranes organize living matter by compartmentalization. They interact with, transport, and are permeable to substrates. Membranes are involved in biosyntheses, energy transduction, information transmission, and cell recognition.[1-3] They define the

0009-2665/87/0787-0877$06.50/0

very existence of the cell. The intense desire to understand the structure of membranes and the mechanisms of their functioning is not surprising. Insight, in the past 80 years, has been gained from studies of biomembranes and/or their constituents in vivo and in vitro as well as from the examination of a variety of membrane models.[4] Investigations of models have led to the rationalization of many properties, including osmotic activity, phase transition, phase separation, dissymmetry, fluidity, permeability, fusion, and sub- and supramolecular mobilities, in and on membranes. There are, of course, no perfect models, and no single model can faithfully reproduce all of the complexities of the biomembranes.

A subtle, but important, difference is to be noted between modeling and mimicking. Modeling (diminutive of Latin modus = form) implies a more or less faithful duplication of the original in a scaled-down version, whereas mimicking suggests only the imitation of the essential features (Greek mimetikos = imitative, from mimeithai = to imitate). Our concern has been membrane mimetics rather than membrane modeling. No attention has been paid, therefore, to the faithful duplication or reconstitution of cell membranes. The approach of membrane mimetic chemistry has been compared with impressionist paintings. Only the essential components of membranes are placed on the chemist's canvas. Our often-quoted motto has cautioned against the slavish and needless copying of mother nature. Membrane mimetic chemistry is distinctly utilitarian. The purpose is not "to obtain a better understanding" of the biomembrane but to develop new approaches and to find solutions to practical problems.[5-7]

Surfactant assemblies whose properties are well understood at the chemical level are used to mimic the desired functions of cells membranes. Compartmentalization of molecules in these membrane mimetic systems may alter ground, transition, and product states and could reduce reaction dimensionalities. These, in turn, often lead to reaction rates, products, and stereochemistries that are different from those observed in dilute aqueous solutions. Membrane mimetic effects on reaction parameters are well documented.[5,8]

A comparison of natural photosynthesis with sacrificial water photoreduction, mediated by polymerized, surfactant vesicle entrapped, colloidal, catalyst-coated semiconductors, is, perhaps, the best illustration of philosophy of approach in membrane mimetic chemistry (Figure 1).[9-14] In the artificial system, a polymerized surfactant aggregate is used instead of the thylakoid membrane. Energy is harvested by a semiconductor rather than by photosystem I and photosystem II. Electron transfer is rather simple. In spite of these differences, the basic principles are similar. Components of *both* the natural and the artificial systems are compartmentalized. The sequences of events are identical in the two systems: energy harvesting, vectorial charge separation, and reduction.

III. Membrane Mimetic Systems

Any substance capable of compartmentalization and/or accepting molecular guests can be viewed as membrane mimetic. Zeolites, cyclodextrins, crown ethers, and their analogues, as well as the more dynamic

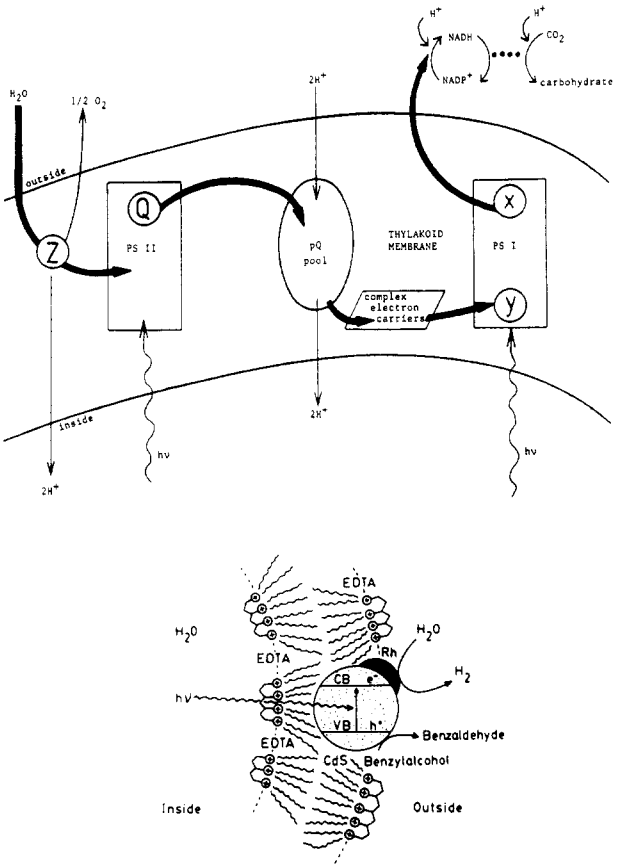

Figure 1. Comparison of grossly oversimplified schemes for natural photosynthesis and sacrificial water reduction in polymerized vesicles. Natural photosynthesis is best understood in terms of the zigzag, or Z, scheme. Briefly, light is harvested by photosystem I (PS I) and photosystem II (PS II). These two systems operate in series; two photons are absorbed for every electron liberated from water. Light-induced charge separation in PS II leads to the formation of a strong oxidant, Z^+ (E_0 = +0.8 V), and a weak reductant, Q^- (E_0 = 0 V). Although the reduction potential of Z^+ is sufficient for water oxidation, evolution of molecular oxygen demands the accumulation of four positive charges. Electrons flow from Q^-, via a pool of plastoquinones (PG) and other complex carriers, to a weak oxidant, y (E_0 = +0.4 V), generated along with a strong reductant, x^- (E_0 = −0.6 V), in PS I. This electron flow is coupled to the $NADH^+ \leftrightarrow NADH$ cycle (via ferrodoxin). Protons enter the ATPase to react with ADP to form ATP (not shown). With the aid of ATP (not shown), x^- reduces CO_2 to carbohydrates. In the mimetic system, water (rather than CO_2) is reduced in the reduction half-cycle to hydrogen at the expense of benzyl alcohol. The local of the CdS/Rh particle is based on chemical experiments.

surfactant assemblies, can all be considered to mimic membranes.[5] Discussion is limited in the present review to selected systems formed from surfactants.

Surfactants, amphiphiles, or detergents are molecules with distinct hydrophobic and hydrophilic regions. Depending on their chemical structures they can be neutral [e.g., polyoxyethylene(9.5)octylphenol (Triton X-100)], cationic [e.g., hexadecyltrimethylammonium bromide (CTAB)], anionic [e.g., sodium dodecyl sulfate (SDS)], and zwitterionic [e.g., 3-(dimethyldodecylammonio)propane-1-sulfonate]. The hydrophobic part of the surfactant can be of various lengths (typically 8–20 carbon atoms), contain multiple bonds, or consist of two [e.g., dioctadecyldimethylammonium chloride (DODAC) dihexadecyl phosphate (DHP)] or more hydrocarbon chains. Surfactants have also been functionalized to contain desired reactive and/or reporter groups. Aggregation behavior depends on the nature

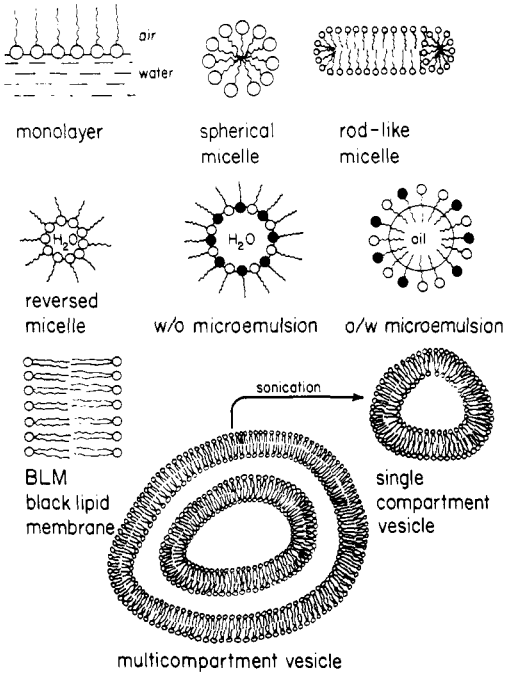

Figure 2. Oversimplified representation of organized structures formed from surfactants.

and the concentration of the surfactants, the nature of the solvent, and the method of preparation. Figure 2 shows a schematic diagram of the most common surfactant assemblies.

In water, 50–100 surfactant molecules, above a characteristic concentration [the critical micelle concentration (CMC)], dynamically and spontaneously associate to aggregates known as micelles.[5,15] Formation of aqueous micelles is a cooperative process. Opposing forces of repulsion between the polar head groups and association between the hydrophobic chains of the surfactants are responsible for micellization. In general, the longer the hydrocarbon tails, the lower the CMC. Aqueous micelles are the most disorganized organized surfactant assemblies. They rapidly break up and reform by two known processes. The first occurs on the microsecond time scale. It releases a single surfactant from the micelle and subsequently reincorporates it. The second process occurs on the millisecond time scale and is due to (a) the dissolution of the micelle and (b) the subsequent reassociation of the monomers.

Increasing the concentration of the surfactant leads to the formation of rodlike micelles and, subsequently, to liquid crystals.

Surfactants having an appropriate hydrophobic lipophilic balance [e.g., sodium bis(2-ethylhexyl)sulfosuccinate (AOT)] undergo self-association in apolar solvents. A useful property of hydrocarbon-soluble surfactants is that they are able to solubilize a large number of water molecules. For example, 1 molecule of AOT is able to solubilize up to 60 molecules of water in a hydrocarbon solvent. Surfactant-solubilized water pools in the hydrocarbon solvent are referred to as reversed or inverted micelles.[16-20] Increasing the concentration of the surfactant-entrapped water, i.e., the size of the water pools, at a given surfactant concentration results in the formation of water-in-oil (w/o) microemulsions. The hydrodynamic diameters of w/o microemulsions are strongly dependent on the temperature. Reversed micelle entrapped water pools are unique. At relatively small water to surfactant ratios (w values, where w = 8–10), all water molecules are strongly bound to the surfactant head groups and cannot be frozen. These immobilized water pools provide the medium for very large and highly specific rate enhancements and resemble the hydrophilic pockets of enzymes.[11]

Spreading an organic solution of a surfactant or phospholipid on water leads to monolayer formation at the water–air interface.[21] Spreading is accomplished in a Langmuir trough, which controls the surface area and surface pressure. Scrupulous cleanliness is a must in monolayer studies. Dipping a dry plate or glass through the monolayer results in the transfer of the surfactant to a solid support. Successive dipping in and out of a monolayer-covered liquid leads to the buildup of multilayers or Langmuir–Blodgett (LB) films.[22] Depending on the mode of dipping, plate–tail–head–tail–head (X-type multilayers), plate–tail–head–head–tail (Y-type multilayers), or plate–head–tail–head–tail (Z-type multilayers) arrangements can be realized. More recently, monolayers have been formed by adsorbing surfactants on the polar solids, typically via silination. Appropriate chemical treatments allow the buildup of successive multilayers.[23] Monolayers are ideal media for investigating two-dimensional processes.

Bilayer (black) lipid membranes (BLMs) are formed by brushing an organic solution of a surfactant (or lipid) across a pinhole (2–4-mm diameter) separating two aqueous phases.[24] Alternatively, BLMs can be formed from monolayers by the Montal–Mueller method.[25,26] In this method, the surfactant, dissolved in an apolar solvent, is spread on the water surface to form a monolayer below the Teflon partitioning, which contains the pinhole (0.1–0.5-mm diameter). Careful injection of an appropriate electrolyte solution below the surface raises the water level above the pinhole and brins the monolayer into apposition to form the BLM. An advantage of the Montal–Mueller method is that it permits the formation of dissymmetrical BLMs. The initially formed film is rather thick and reflects white light with a gray color. Within a few minutes the film thins and the reflected light exhibits interference colors that ultimately turn black. At that point, the film is considered to be bimolecular (40–60-Å thickness). BLMs have been utilized extensively in the elucidation of transport mechanisms by electrical measurements.

Closed bilayer aggregates, formed from phospholipids (liposomes) or from surfactants (vesicles), represent one of the most sophisticated models of the biological membrane.[5,27] Swelling of thin lipid films in water results in the formation of onionlike multilamellar vesicles (MLVs) of 1000–8000-Å diameter. Sonication of MLVs above the temperature at which they are transformed from a gel to a liquid (phase-transition temperature) leads to the formation of fairly uniform single bilayer vesicles of 300–600-Å diameter [small unilamellar vesicles (SUVs)]. SUVs can also be prepared by injecting an alcohol solution of the surfactant through a small-bore syringe into water, by detergent dialysis, or by gel filtration. Uniform SUVs can be obtained by ultracentrifugation and by membrane or gel filtration. Both SUVs and MLVs undergo temperature-induced phase transitions. At low temperature, phospholipids are arranged in tilted, one-dimensional lattices. At tem-

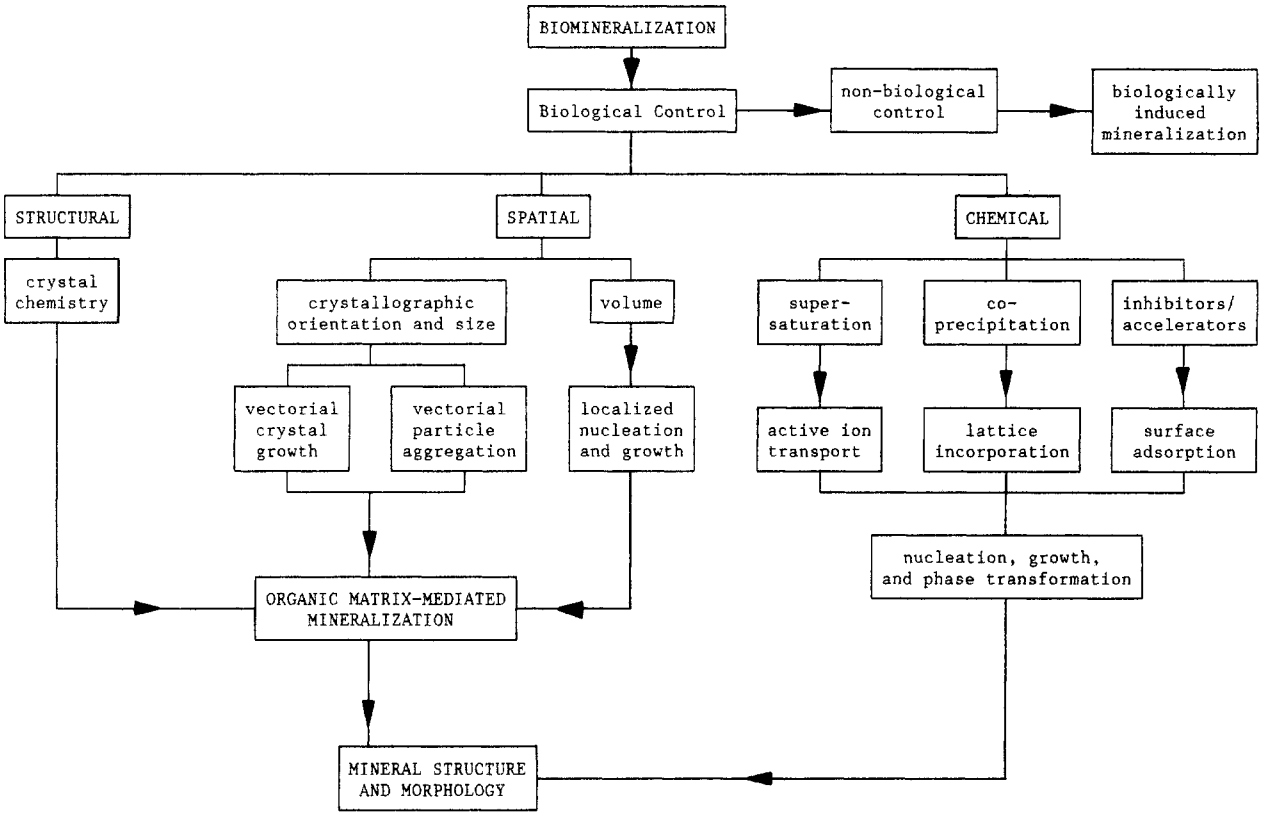

Figure 3. General scheme for biological control in mineralizing systems. Reproduced with permission from ref 34 (copyright 1983, Springer).

peratures just below the transition, two-dimensional arrangements form. Above the main phase-transition temperature, phospholipids revert to one-dimensional arrangements, separated somewhat from each other, and assume liquidlike configurations. The kinetic stability of vesicles is considerably greater than that of micelles. There is no equivalent of a critical micelle concentration. Once formed, vesicles cannot be destroyed by dilution. Typically, they are stable for weeks. Their stability can be enhanced further by polymerization. Vesicles have a large number of solubilization sites. Hydrophobic molecules can be distributed among the hydrocarbon bilayers of the vesicles. Polar molecules may move about relatively freely in vesicle-entrapped water pools, particularly if they are electrostatically repelled from the inner surface. Small charged ions can be electrostatically attached to the oppositely charged outer or inner surfaces of vesicles. Species having charges identical with those of the vesicles can be anchored onto the vesicle surface by a long hydrocarbon tail.

Polymerized surfactant vesicles have become the most sophisticated systems in the armory of membrane mimetic chemists.[28-31] The need for increased stabilities and for controllable permeabilities and morphologies led to the development of polymerized surfactant vesicles. Vesicle-forming surfactants have been functionalized by vinyl, methacrylate, diacetylene, isocyano, and styrene groups in their hydrocarbon chains or at their head groups. Accordingly, surfactant vesicles could be polymerized in their bilayers or across their head groups. In the latter case, either the outer or the inner vesicle surfaces could be linked separately. All polymerized vesicles show appreciable stabilities compared with their unpolymerized counterparts. They have extensive shelf lives and remain unaffected by the addition of up to 30% alcohol. Monolayers, LB films, and, more recently, BLMs have also been polymerized.[28-31]

Table I summarizes the most important properties of surfactant assemblies utilized in membrane mimetic chemistry.

IV. Clustering in Biomembranes—Biomineralization

Precipitated and/or clustered inorganic compounds play important roles in biology.[32,33] They are part of the bone structure and teeth and are involved in storage and direction finding as magnetic and gravity devices. These latter functions require extremely fine spatial and geometrical tuning of the clusters. Biological control of inorganic cluster formation—biomineralization—is largely mediated by cellular membranes.

The physical–chemical bases for biomineralization have only been examined recently.[34-37] Figure 3 reproduces the proposed scheme for structural, spatial, and chemical controls of biomineralization. Structural and chemical controls have been rationalized in terms of known solid-state, colloidal–chemical, and crystallographic principles. Thus, the availability of appropriate precursors in appropriate concentrations and the presence of a matrix determine the outcome of nucleation (in precipitation or coprecipitation processes) and particle growth.[39,40]

Compartmentalization provided by membranes and cells is responsible for the inflow of ionic precursors and imposes size and shape limits on particle growth. Interaction with the cell matrix can also influence the orientation of crystal growth. Lipid vesicles often act as molecular transporters between cells.

TABLE I. Properties of Organized Surfactant Assemblies

	aqueous micelles	reversed micelles	microemulsions	monolayers	BLMS	vesicles
method of preparation	dissolving appropriate (above the CMC) concentration of the surfactant in water	dissolving appropriate concentration of the surfactant in an apolar solvent and adding small amounts of H_2O	dissolving appropriate concentrations of the surfactant and cosurfactant in water or in oil	spreading the surfactant (or a dilute solution of it in an organic solvent) on water surface	painting a dilute surfactant on a Teflon pin hole	shaking thin films of lipids (or surfactants in water, or ultra-sonication, of alcohol injection, or detergent dilution
weight-averaged MW	2000–6000	2000–6000	10^4–10^7	depends on area covered and density of coverage	depends on area covered and density of coverage	$>10^7$
hydrodynamic diameter, Å	40–100	40–100	50–5000	depends on area covered and density of coverage	depends on area covered and density of coverage	300–10 000
time scale of monomer aggregate formation, break-down	10^{-4}–10^{-6} s	10^{-4}–10^{-6} s	10^{-4}–10^{-6} s	monomer to subphase, minutes–hours	monomer to plateau border, minutes	monomer to bulk, minutes–hours
stability	months	months	months	days, weeks	hours	weeks–months
dilution by H_2O	destroyed	water pools, enlarges: w/o microemulsions formed	depends on the phase diagram			unaltered
number of reactants solubilized per aggregate	few	few	large	large	large	large
solubilization sites	distributed around and within the Stern layer; no "deep penetration"	aqueous inner pool, inner surface, surfactant tail	inner pool, inner surface, surfactant tail	intercalation and surface	either or both sides of the bilayer or within the bilayer	inner pool, inner, outer surface, bilayer

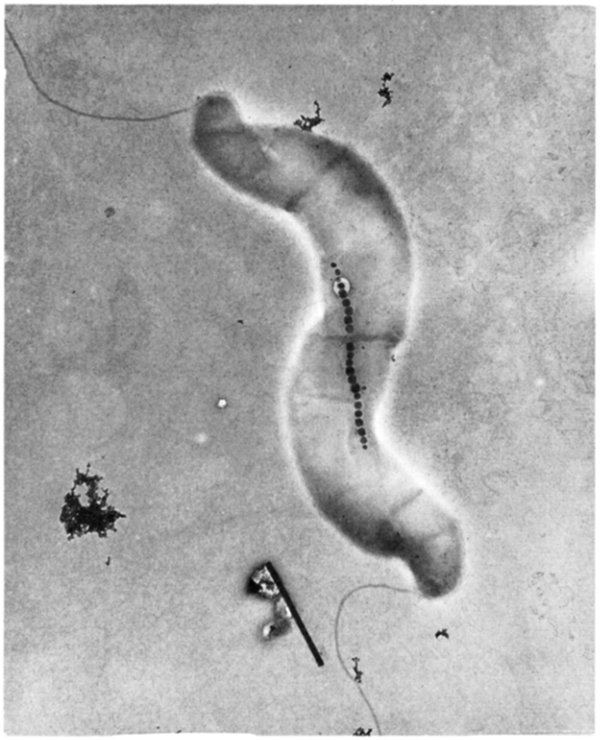

Figure 4. Electron micrograph of particle chain in magnetotactic bacteria. Reproduced with permission from ref 41 (copyright 1986, Rockefeller University Press).

Magnetic bacterium (*Aquaspirillum magnetotactitum*) is the living example of stringent biomineralization[42] (Figure 4).[41] Typically, each organism contains 20–25 45 ± 8 nm diameter, spherical, single-domain Fe_3O_4 (magnetite) particles, which are longitudinally aligned in the cytoplasmic membrane. This precise molecular organization imparts a magnetic moment parallel to the axis of motility. Magnetic bacteria manage to swim downward in both the northern and southern hemispheres! Our challenge is to discover the chemistry this species utilizes for manufacturing and packaging its navigational device.

V. Quantum Size Effects

Ultrasmall (50-Å-diameter and less) colloidal particles have, until recently, been the modern equivalent of Ostwald's[43] "world of neglected dimensions".[44] Colloidal particles of these dimensions are inherently interesting, since they can provide information on the physical and chemical consequences of transition between individual molecules, molecular clusters manifesting cooperativity, and bulk materials. The intense current scrutiny of these systems has been prompted by the many unique properties they manifest at the region of cluster formation.

Size effects have been investigated on dispersed colloidal semiconductors.[45–50] Initial decrease in the size of dispersed colloidal semiconductors (40–60-Å diameter for CdS or ZnS) results only in a decrease in the density of states in the conduction band and, hence, in the absorption coefficient. Until the exciton state, lying just below the edge of the conduction band, is not appreciably affected, a decrease in the semiconductor size will only be manifested in a modest ultraviolet shift of the absorption. Development of a shoulder at the blue edge of the band gap corresponds to an electronic transition

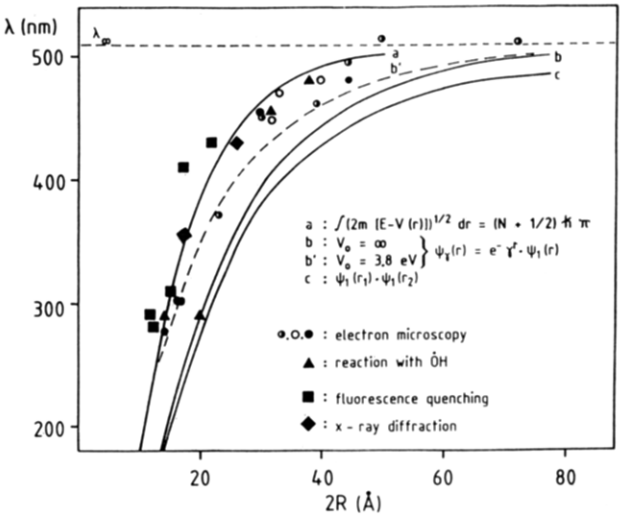

Figure 5. Wavelength $\lambda_{threshold}$ as a function of diameter $2R$ of CdS particles. λ_∞ is the wavelength for macrocrystalline material. Key: points, experimental data; curves, calculated. See text for details. Reproduced with permission from ref 54 (copyright 1986, Elsevier).

from the valence band to the exciton state. Further decreases in the semiconductor size lead to ultrasmall particles in which the charge carriers are confined in a small volume. Band gaps of semiconductors in this "Q-state" are shifted dramatically to higher energy. It has been possible, for example, to prepare colorless dispersed CdS colloids.[44]

Quantum size effects have been treated theoretically by several methods.[51–54] The simplest model utilized the one particle in the box approach.[53] The exciton [consisting of a conduction-band electron (e^-) and a valence-band hole (h^+)] was considered as an electron moving at a reduced mass, $\mu = (1/m_{e^-} + 1/m_{h^+})^{-1}$, around a fixed h^+. Curve a in Figure 5 gives the lowest energy transition calculated for this model by the semiclassical approximation.[53] Accurate quantum mechanical calculations of the energy spectrum of the same model resulted in curve b in Figure 5 for the lowest energy transition.[54] Curve b′ in Figure 5 was assessed by using the actual potential energy difference between the lower edge of the conduction band of the macrocrystal and the vacuum level ($V_0 = 3.8$ eV) rather than $V_0 = \infty$ (hard-sphere approximation).[54] A more rigorous two body (m_{e^-} and m_{h^+}) in the box model was used in the quantum mechanical calculation of the lowest eigenstate of the Wannier exciton.[51,52] Curve c in Figure 5 gives the absorption edge as a function of the diameter ($2R$) of the CdS semiconductor according to this calculation. Figure 5 compares experimentally determined and theoretically obtained relationships between the absorption edge and the CdS particle diameters. Experimental values were obtained from X-ray diffraction and electron microscopic measurements, as well as inferred from kinetic determinations of the rates of interactions with hydroxyl radicals and with fluorescence quenching studies in the presence of methylviologen.[54]

The significance of quantum size effects is well illustrated by the altered redox potentials of semiconductors. Band-gap irradiation of CO_2-saturated solutions of dispersed colloidal CdSe particles with diameters smaller than 50 Å produced formic acid. Conversely, excitation of larger CdSe particles under iden-

tical conditions did not result in formic acid production.[55]

VI. Rationale for Mimetic Approach

Stripping away the complexities, the essential requirement of biomineralization is to have compartments capable of providing structural, spatial, and chemical controls for cluster generation and stabilization. Compartmentalization in membrane mimetic systems duplicates this requirement well. The tenet of this review is that the mimetic approach allows the formation of controlled-size, uniform, and stable particles and thus opens the door to many innovative applications.

It is important to select a given membrane mimetic system for a given application. Sizes, morphologies, microenvironments, and kinetic stabilities are factors to be considered. Aqueous micelles are spherical entities having 30–60-Å diameters. Reversed micelles have similar dimensions. Micellar dimensions can appreciably increase upon the solubilization of large molecules. Microemulsions and vesicles are considerably larger than micelles. Their diameters range from 50 to 1000 Å and from 300 to 5000 Å, respectively. Consequently, w/o microemulsions contain considerably larger water pools than reversed micelles. Dimensions of monolayers depend on the surface area of the subphase and on the surface pressure, and BLMs are confined within a relatively small pinhole. Micelles are in dynamic equilibrium with monomeric surfactants. Behavior of microemulsions is quite analogous. Conversely, surfactant residence times in vesicles are on the order of minutes to hours. Micelles, microemulsions, and vesicles can remain stable for weeks subsequent to their formation. Monolayers, under appropriate conditions, can be kept for an equally long time. BLMs, however, rarely last longer than a couple of hours.

Phase transition is an important property of monolayers, BLMs, and vesicles. Depending on the surface area–pressure isotherm, monolayers may be in a gaseous, fluid, or solid state. Thermotropic phase transitions of BLMS and vesicles involve changes in the arrangements of lipids without altering the gross structural features of the bilayers. Below the phase-transition temperature, the surfactant constituents of BLMs and vesicles are in highly ordered "solid" states, with their alkyl chains in all-trans conformations. Above the phase-transition temperature, lipids become "fluid" as the result of gauche rotations and kink formation. Micelles and host systems do not have temperature-induced phase transitions (micelle formation requires molten chains). There are additional motions of surfactants within the BLMs and vesicles. Surfactants may undergo segmental and rotational motions, lateral diffusion, and flip–flop.

Micelles, microemulsions, monolayers, organized multilayer assemblies, BLMs, vesicles, hosts, and polyelectrolytes provide regions of different polarities, acidities, and viscosities. Most substrates are solubilized at the micellar head-group region at a microenvironment that resembles that of alcohols. There is a considerable amount of bound water at the inner surface of reversed micelles. By varying the size of the surfactant-entrapped water pool, effective polarities of the environments can be substantially altered. Thus, water in reversed micelles can attain polarities corresponding to that of benzene. W/o microemulsions are expected to provide environments similar to those of reversed micelles. Monolayers provide relatively polar environments close to their head groups. Environments around the hydrocarbon tails depend on the surface pressure, that is, on the proximity of monolayer-constituting surfactant molecules to each other. Vesicle bilayers are not as flexible as monolayers. They provide considerably more rigid interiors than micelles. Rigidities of bilayers can be further increased by the addition of cholesterol. Vesicle-entrapped water pool(s) provide additional unique environments. Since proton permeabilities across vesicle walls can be drastically reduced, it is possible to maintain substantial pH gradients between vesicle-entrapped and bulk water for several hours. Vesicles are osmotically active. In hyperosmolar solutions they shrink, and in hypoosmolar solutions they swell. An important consequence of osmotic shrinkage is that all of the liposome-entrapped water becomes bound to the head groups located at the inner surface of the vesicle.

Ionizable membrane mimetic agents behave quite differently from simple electrolytes in dilute aqueous solutions. Micelles, monolayers, BLMs, and vesicles have appreciable surface potentials and charge densities. Charge distribution is treated by the various electrical double-layer theories. One important result is that negatively charged membrane mimetic agents attract positive counterions, while positively charged membrane mimetic agents attract positive counterions, while positively charged ones are surrounded by negative counterions. Consequently, the surface pH of anionic membrane mimetic agents is lower than that of the bulk solution. The reverse trend is observed for cationic membrane mimetic agents. The very nature of BLMs and vesicles allows the establishment of potential gradients across their bilayers.

The most likely substrate solubilization sites in micelles and microemulsions are the interface and Stern regions. There is no evidence for "deep" substrate penetration into the micellar core.

Substrates can penetrate into the hydrophobic regions of monolayers or associate with their head groups. They can migrate laterally and, indeed, across monolayers in organized multilayer assemblies.

The considerable kinetic stabilities of BLMs and vesicles govern the dynamics of substrate interaction in these systems. Even the terminology is different from that used in micelles. Permeabilities and diffusion rates rather than residence times are determined. Substrate permeabilities are relatively slow. The time scale for the transport of water molecules across liposomes is on the order of seconds. Diffusion of larger molecules through liposomes occurs on the time scale of hours, days, and even weeks.

Microemulsions, vesicles, and, more recently, LB films and BLMs have been utilized as compartments for microcrystals, catalysts, semiconductors, and magnetic particles. Details of these investigations will be examined in the ensuing discussion.

VII. Precipitation and Crystallization in Mimetic Membranes

Colloidal particle formation is a complex process.[56] It involves a delicate interplay between nucleation,

TABLE II. Precipitation in Mimetic Membranes

membrane mimetic system	incorporated particle(s)	results	ref
(i) AOT (0.2 M)–heptane–H_2O reversed micelle, [AOT]:[H_2O] = 8:1 (ii) nonionic Ukanil 25 (poly(ethylene oxides), 0.2 M)–heptane–H_2O reversed micelle	AgCl prepared by mixing equal vol of $AgNO_3$ and NaCl containing reversed micelles	turbidity, X-ray diffraction, and small angle X-ray syncrotron scattering measurements indicated monodisperse 60-Å AgCl particles within a few minutes; subsequent growth (flocculation) very slow; same particles formed in i and ii	57
sodium dodecyl sulfate–isopropyl alcohol–benzene–H_2O w/o microemulsion	AgCl prepared by mixing equal volumes of $AgNO_3$ and NaCl containing w/o microemulsions	rates of AgCl formation, determined by stopped flow spectroscopy, depend on microemulsion structure	58
poly(oxyethylene ether)–cyclohexane (or isooctane)–H_2O w/o microemulsion	fine $BaCO_3$ particles prepared by bubbling CO_2 into $Ba(OH)_2$ containing microemulsion	particle size depends on microemulsion composition	59
AOT–cyclohexane–H_2O w/o microemulsion	monodisperse $CaCO_3$ particles prepared by bubbling CO_2 into $Ca(OH)_2$ containing microemulsion	particle size depends on microemulsion composition	60
sorbitan monooleate (SPAN-80)–2-ethylhexanol–water w/o microemulsion	Fe_2O_3 particles prepared	morphology and ratio of α-Fe_2O_3 to γ-Fe_2O_3 depend on microemulsion composition	61
egg yolk phosphatidylcholine single bilayer 30–60-nm-diameter vesicles	monodispersed Ag_2O particles (10.55 ± 1.25 nm) prepared from $AgNO_3$, localized inside vesicles, by OH^-; intravesicular AgCl and AgS also formed	mechanism of intravesicular precipitation discussed	62–66
single bilayer 20-nm-diameter phosphatidylcholine vesicles	CoS particles precipitated from $CoCl_2$, localized inside vesicles by $(NH_4)_2S$	vesicle-entrapped species aid NMR spectroscopy	62, 66
egg yolk phosphatidylcholine single bilayer 30–60-nm-diameter vesicles	amorphous FeO(OH) and $CoSiO_3$, and crystaline Ag_2SiO_3	X-ray microprobe analysis used to characterize the systems	66, 67

microcrystal formation, intermediate growth (Ostwald ripening), coagulation, and flocculation. Much of our understanding has been obtained by investigating simplified systems in isolation. Typically, this involved the addition of surfactants as stabilizing or coagulating agents. Confinement in a mimetic system inherently limits particle growth and, hence, simplifies the colloid chemistry. Indeed, precipitation in microemulsions and vesicles, summarized in Table II, has provided fundamental insights into these processes in addition to offering a new approach for obtaining controlled-size, monodispersed particles.

The recognized importance of AgCl microcrystals in photography has prompted their investigation in mimetic systems.[57,58] Significantly, confinements of AgCl in microemulsions inhibited Ostwald ripening. Addition of surfactants subsequent to mixing the $AgNO_3$ and NaCl containing microemulsions, mixing nonstoichiometric amounts of Ag^+ and Cl^- ions, and the use of nonionic microemulsions have resulted in enhanced stabilization of the AgCl microcrystals.[57] Rate constants for AgCl coagulation in microemulsions, relative to that in water, k_{rel}, were found to depend markedly on the microemulsion composition.[58] Enhanced k_{rel} values corresponded to a region of the microemulsion dominated by the polar solvents (water and alcohol) and, hence, to the presence of normal and reversed micelles. Electrostatic repulsions between the charged micelles is a factor that limits the growth of AgCl. Micellar growth occurs concomitantly with AgCl coagulation.[58]

Precipitation in vesicles leads to uniform particles (Figure 6)[63] that remain stable as long as vesicle fusion and internalization is precluded. Utilization of polymer-coated and polymerized vesicles can lead to unprecedented stabilities.[28–31]

Crystalline Ag_2O formation in vesicles represents the earliest example of deliberate mimicking of biomineralization.[62,63] $AgNO_3$ was entrapped into egg yolk phosphatidylcholine vesicles by sonication at pH 5.0. External silver ions were removed by a passage through a cation-exchange resin. Raising the solution to pH 12.0–12.6 resulted in the transvesicular passage of hydroxide ions and, hence, the precipitation of Ag_2O. Electron microscopy indicated that nucleation of Ag_2O occurred only at one site. Conversely, $Co(OH)_2$ precipitation was proposed to be the consequence of multisite nucleations. Figure 7 illustrates these different intravesicular precipitation mechanisms.[63] Intravesicular Ag_2O precipitation was discussed in terms of a diffusion-controlled, hydroxide ion permeation,

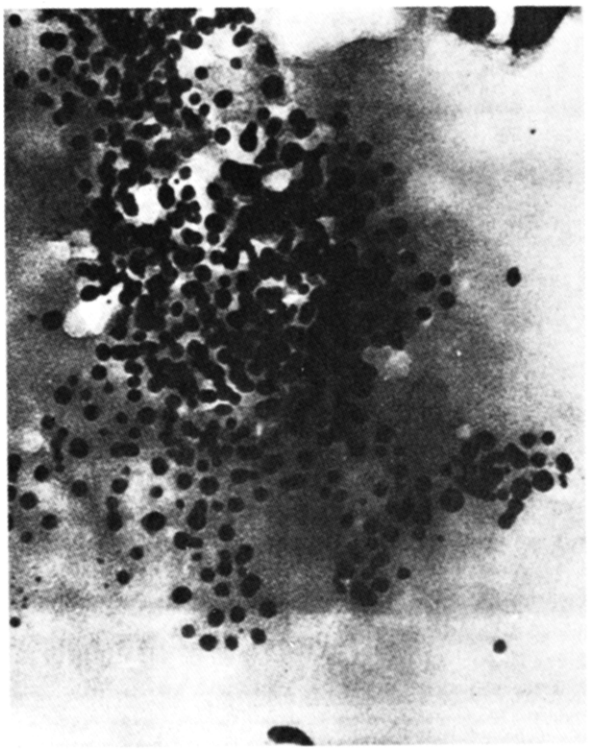

Figure 6. Electron micrograph of intravesicular Ag_2O particulates, 286 000×. Reproduced with permission from ref 63 (copyright 1983, Royal Society of Chemistry).

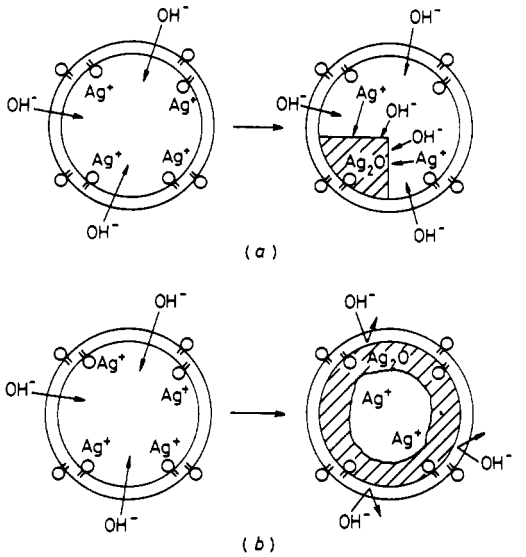

Figure 7. Possible mechanisms of Ag_2O nucleation within vesicles: (a) nucleation at a single site; (b) nucleation at several sites along the vesicle membrane. Reproduced with permission from ref 63 (copyright 1983, Royal Society of Chemistry).

followed by a rate-determining crystallization (eq 1 and 2), where the subscripts in and out refer to vesicle in-

$$OH^-_{out} \rightarrow OH^-_{in} \quad (1)$$

$$2OH^-_{in} + 2Ag^+_{in} \rightarrow Ag_2O_{in} + H_2O \quad (2)$$

terior or exterior. The rate of precipitation, R, and those at time t, R_t, were given by eq 3, where K_{sp} is the

$$R = K(\text{supersatn})^x$$
$$R_t = K[Ag^+]_{in,t}[OH^-]_{in,t} - K_{sp} \quad (3)$$

solubility product of Ag_2O. The observed rate was found to be first order with respect to $[OH^-]_{out}$ in the pH 11.0–12.0 region and first order with respect to $[Ag^+]_{in}$. Maintaining supersaturation was found to be essential for Ag_2O formation. A low level of supersaturation, obtained at a slow rate of OH^- influx, limited the nucleation sites and, hence, controlled crystal growth.[63]

These pioneering works on controlled crystallization in mimetic membranes will pave the way to many additional studies leading to important technical utilizations.

VIII. Catalysts in Mimetic Membranes

Catalytic efficiency and selectivity depend, to a large extent, on the surface area and geometry of the catalyst.[68] Excluding other factors, the larger the catalytic area, the more efficient is the catalyst.[68-70] Development of small, uniform catalyst particles with controllable morphologies and their deposition on a solid support without aggregation have been major scientific and engineering challenges.[71] The approaches taken included vacuum and molecular depositions,[72] radiation,[73] and classical colloid chemical techniques.[74] Membrane mimetic systems provide a viable alternative for generating monodisperse, small catalytic clusters. Under ideal conditions, catalytic clusters show long-term stability in the mimetic membranes and are completely

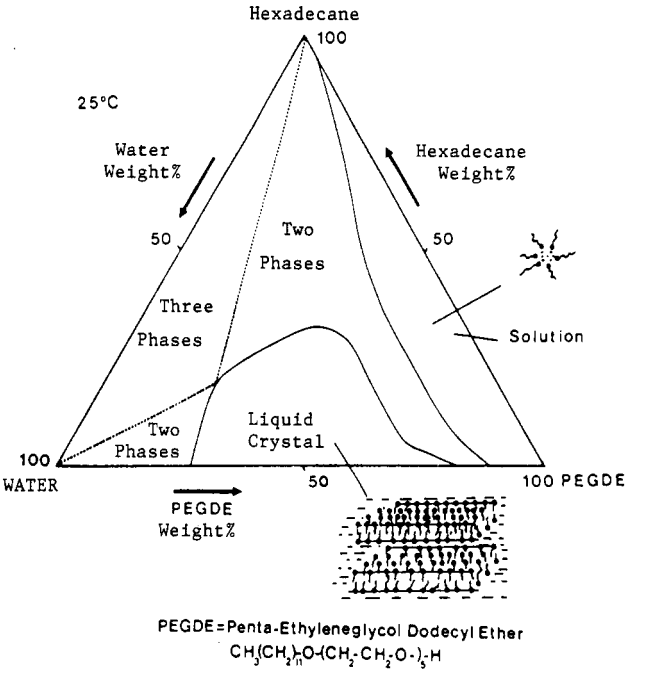

Figure 8. Phase diagram for the three-component system water–pentaethylene glycol dodecyl ether (PEGDE)–hexadecane at 25 °C. Reproduced with permission from ref 75 (copyright 1982, Elsevier).

accessible to reacting molecules (bubbling gases through a well-constructed catalytic cluster carrying w/o microemulsions, for example). This situation would lead to considerably greater surface areas and, hence, to catalytic contacts greater than could be realized for catalysts deposited on solid surfaces. Available information on generating catalytic clusters in mimetic systems and utilizing them is summarized in Table III.[75-88]

Extremely small (<10-nm-diameter) monodisperse Pt, Pd, Rh, and Ir particles were prepared in situ in the aqueous pools of w/o microemulsions.[75-77] Microemulsions were selected that had well-characterized, closed, and moderately sized aqueous compartments whose structures and chemical compositions remained unaffected by the introduction of appropriate metal ions and reducing agents. Examination of phase diagrams (see, for example, that for pentaethylene glycol dodecyl ether (PEGDE)–hexadecane–H_2O in Figure 8) aided the selection of the most suitable microemulsion systems. Subsequent to their introduction, the metal salts were reduced by hydrogen or hydrazine. Remarkably uniform (3.0 ± 0.3 nm diameter) Pt particles were obtained by reduction of different amounts of H_2PtCl_6 in situ in PEGDE–hexane–water microemulsions by hydrazine.[75] Significantly, the microemulsion-entrapped catalyst clusters remained stable for several months. An important advantage of generating uniformly sized, small catalytic particles in microemulsions is that they can be transferred to solid support without agglomeration by evaporating the organic solvent.[75] Thus, deposition of microemulsion-generated platinum particles on solid support provided an excellent catalyst for but-1-ene hydrogenation and isomerization. Considerably less catalytic efficiency was observed, however, on performing the same reaction in the microemulsion phase.[76,77] Apparently, surfactant coating hindered the accessibility of but-1-ene and hy-

TABLE III. Catalysts in Mimetic Membranes

membrane mimetic system	incorporated particle(s)	results	ref
(i) pentaethylene glycol dodecyl ether (PEDGE)–hexadecane (or hexane)–H_2O w/o microemulsion (ii) hexadecyltrimethylammonium chloride (CTAB)–octanol–H_2O w/o microemulsion (iii) sodium octanoate–decanol–H_2O w/o microemulsion	monodisperse 3–5-nm-diameter Pt, Pd, Rh and Ir particles prepared by in situ reduction of their metal salts in i–iii w/o microemulsions	method generally applicable if (i) salt is soluble, (ii) reducing agent only reacts with salt, and (iii) temperature is appropriate	75
(i) pentaethylene glycol dodecyl ether (PEDGE)–hexadecane (or hexane)–H_2O w/o microemulsion (ii) hexadecyltrimethylammonium chloride (CTAB)–octanol–H_2O w/o microemulsion (iii) polyethylene sorbitane tristearate (Tween 65)–hexane–decane–H_2O reversed micelle (iv) Tween-65 alcohol surfactant solution	monodisperse 2–3-nm-diameter Pt and Rh, and 5-nm-diameter Pd particles prepared by in situ reduction of their metal salts in i–iv	efficiency of Pt, Rh, and Pd as catalysts in i–iv microemulsions examined for: but-1-ene $\xrightarrow[H_2\ (or\ Du)]{catalysts}$ butane (hydrogenation); *trans*-but-2-ene (isomerization); *cis*-but-2-ene (isomerization)	76 77
CTAB–hexanol–H_2O reversed micelles	monodisperse nickel boride prepared by $NaBH_4$ reduction of Ni^{2+} dissolved in reversed micelles	nickel boride in reversed micelles is a better catalyst than Raney nickel for *n*-1-heptene reduction	78
CTAB–hexanol–H_2O reversed micelles	monodisperse 20–60-Å-diameter cobalt boride prepared by $NaBH_4$ reduction of Co^{2+} disolved in reversed micelles	cobalt boride in reversed micelles is a comparable catalyst to Raney nickel for *n*-1-heptene reduction	79
CTAB–hexanol–H_2O reversed micelles	monodisperse 30–60-Å-diameter iron boride prepared by $NaBH_4$ reduction of Fe^{3+} disolved in reversed micelles	size of micellar core controls particle sizes	80
CTAB–hexanol–H_2O reversed micelles	monodisperse 20–60-Å-diameter cobalt boride prepared by $NaBH_4$ reduction of Co^{2+} disolved in reversed micelles	system characterized by ^{13}C and ^{19}F NMR and absorption spectroscopy	81
pentaethylene glycol dodecyl ether (PEDGE)–hexane–water w/o microemulsion	monodisperse Au particles generated in situ by photolysis of $HAuCl_4$ entrapped in w/o microemulsion	mechanisms of $[Au^0]_n$ formation examined by pulse radiolysis and laser flash photolysis	82
single-compartment 1430-Å-diameter bilayer vesicles prepared from mixtures of dipalmitoylphosphatidylcholine (DPPC) and $[CH_2{=}CH(CH_2)_8COO]_2NPO(OH)_2$ or from mixtures of DPPC and $[H_2C{=}CHC_6H_4NHCO(CH_2)_{10}](C_{16}H_{33})N^+(CH_3)_2,Br^-$	ca. 270-Å colloidal Pt particles generated in situ in vesicles by photolysis of K_2PtCl_4	vesicle-incorporated methylene blue (MB) or 10-methyl-5-deazaisoalloxazine-3-propanesulfonic acid (MAPS) catalytically reduced by bubbling H_2 through Pt-containing vesicles; subsequent extravesicular addition of Fe^{3+} led to Fe^{2+} and MB or MAPS reformation; these steps could be repeated several times	83
single-compartment 1430-Å-diameter bilayer vesicles prepared from mixtures of dipalmitoylphosphatidylcholine (DPPC) and $[CH_2{=}CH(CH_2)_8COO]_2NPO(OH)_2$ or from mixtures of DPPC and $[H_2C{=}CHC_6H_4NHCO(CH_2)_{10}](C_{16}H_{33})N^+(CH_3)_2,Br^-$	ca. 270-Å colloidal Pt particles generated in situ vesicles by photolysis of K_2PtCl_4	vesicle-entrapped or isolated Pt used as catalysts for ethylene and cyclohexene hydrogenation	84
sodium undecanoate aqueous micelle polymerized (to polyelectrolyte)	ca. 1.1-nm colloidal Pt particles generated in situ in micelles by photolysis of K_2PtCl_4	photochemical sacrificial H_2 generation examined on using $EDTA/Ru(bpy)_3^{2+}/MV^{2+}$ in the presence of Pt-containing polymerized sodium undecanoate	85
dodecyltrimethylammonium chloride and sodium dodecyl sulfate aqueous micelles	colloidal Pt particles formed by photolysis of K_2PtCl_4 were protected by micelles	vinyl acetate reduction examined in presence of micelle-stabilized Pt catalyst	86
LB films prepared by depositing 20–25 layers of behemic acid ($C_{21}H_{43}COOH$) on calcium fluoride (3 × 1 cm) plates	LB films immersed in aqueous $AgNO_3$, dried, excess Ag^+ washed away (by H_2O), dried, exposed to hydrazine water to produce 10–20-Å-diameter silver clusters	structures of LB films, silver ions, and silver clusters therein investigated by absorption and infrared spectroscopy, X-ray diffraction, and electron microscopy	87 88

drogen to the catalytic surface. The design of an appropriate mimetic system that stabilizes uniform small catalytic particles without unduly diminishing their effective surface areas remains a worthy challenge!

Monodisperse 20–70-Å-diameter Ni_2B, Co_2B, and $FeB–Fe_2O_3$ particles have been prepared by the in situ reduction of metal salts in CTAB–hexanol–H_2O reversed micelles by $NaBH_4$.[78–81] Metal boride particle formation has been discussed in terms of (i) metal ion compartmentalization in the aqueous pool of microemulsions, (ii) exchange of water contents, (iii) diffusion of $NaBH_4$ to the water pools, (iv) nucleation in pools containing at least two metal ions, (v) particle growth, and (vi) stabilization (Figure 9). The concentration and coordination of the metal ions within the differently sized, surfactant-entrapped water pools influence the mechanism of metal boride formation in reversed micelles. Absorption, electron paramagnetic resonance, and ^{13}C and ^{19}F nuclear magnetic resonance spectroscopic measurements have led to the proposed modes of metal ion coordination in the reversed micelles (Figure 10).[79] In CTAB reversed micelles, one and two

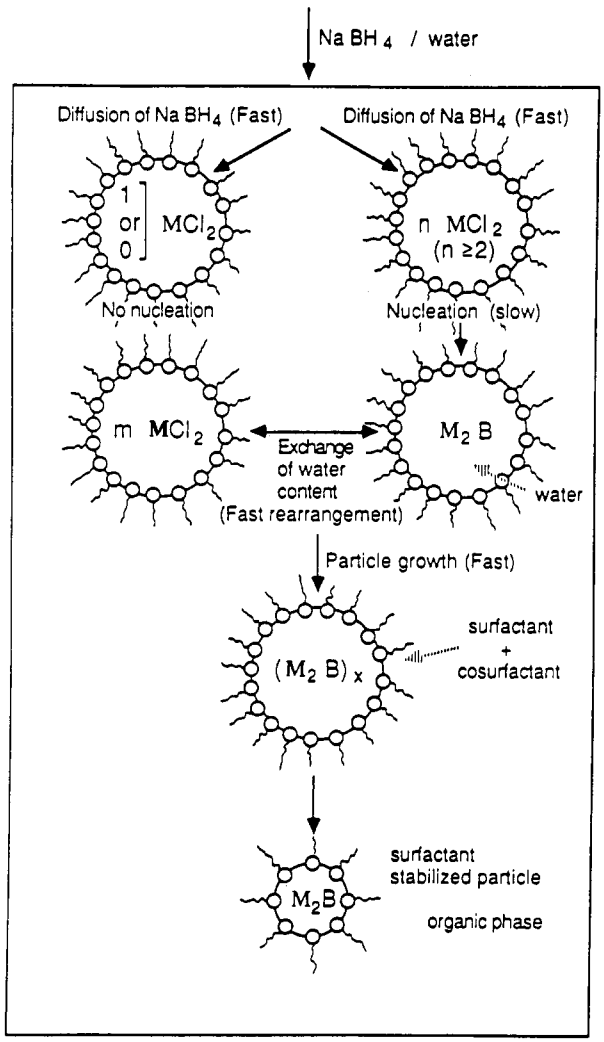

Figure 9. Proposed mechanisms for metal boride formation in reversed micelles. Reproduced with permission from ref 71 (copyright 1986, Plenum Press).

hexanol molecules participate in the coordination shells of the tetrahedral Co and Ni complexes, respectively. No organic solvent was found to participate in the coordination shell of CTAB reversed micelle incorporated iron atoms, and the situation in nonionic Triton X surfactants is completely different (Figure 10).[79] Sizes of boride particles primarily depended on the size of the water pools and on the concentration of metal ions therein. Large metal boride clusters were obtained, as expected, in larger pools at higher precursor concentrations. A satisfactory model has been developed for colloidal cluster formation in w/o microemulsions.[79] The ultimate aim of this work is, of course, the development of efficient catalysts. This has been demonstrated for the reduction of *n*-1-heptene (Table III).[78]

The mechanism of colloidal gold cluster formation in PEGDE–hexane–water w/o microemulsion has been investigated by pulse radiolysis and laser-flash photolysis.[82] Rate constants have been determined for $Au^{3+} + e_{aq}^- \rightarrow Au^{2+}$, $2Au^{2+} \rightarrow Au^{3+} + Au^+$, and $Au^+ + R^{\bullet -} \rightarrow Au_0 + R$ (where $R^{\bullet -}$ is an unidentified radical). On the longer time scale, formation of colloidal gold, $nAu_0 \rightarrow [Au^0)_n$, has been observed. Absorbances of colloidal gold formed in microemulsion were approximately 5 times greater than that in water, even though the aqueous solutions received fivefold more laser doses than the microemulsions. In aqueous $HAuCl_4$ solutions, unlike microemulsions, colloidal gold formation was barely observable subsequent to exposure to laser pulses for 1 min. Since the extinction coefficient of colloidal gold increases with increasing particle size, the higher absorbance in microemulsions (at ca. 150-Å gold particle diameter) than that in water (at ca. 400-Å gold particle diameter) implies the formation of higher concentrations of colloidal gold in microemulsions. Colloidal gold formation is apparently a less efficient process in bulk than in surfactant-entrapped water pools. Further, in microemulsions, the absorption of colloidal gold, formed either in pulse radiolysis or in laser photolysis, has a pronounced maximum at 525 nm. Conversely, in water, the absorption spectrum of colloidal gold is broader, is shifted to longer wavelength, and may be resolved into two maxima. These observations are explicable in terms of the formation of larger colloidal gold particles in water than in microemulsions. Recently calculated extinction cross sections for gold particles of 25–100-Å diameter indicated absorption maxima at 525 nm. Absorption maxima for particles with diameters of 150, 250, and 350 Å shifted to 540, 570, and 640 nm, respectively. On the basis of this calculation, an upper limit of a 150-Å diameter can be placed on the mean sizes of colloidal gold in microemulsions. Rates of growth of colloidal gold are also different in the two media. In water, the absorbance increase is relatively slow and gradual at all wavelengths. Conversely, in microemulsions, absorbances at different wavelengths increase at the same rate in the initial 50 min, after which the absorbances at 530 nm increase at a somewhat greater rate than those at shorter wavelength.

The size of the microemulsion droplet limits the size of gold colloids if Poisson's distribution prevails.[82] Since surfactant-entrapped water molecules exchange on the millisecond time scale, formation of larger colloidal particles is possible by aggregation of neutral gold atoms from different droplets. Growth is ultimately limited by statistical considerations. The rate of reduction has been shown to affect profoundly the morphology, and hence the catalytic efficiency, of colloidal metal particles. High-energy laser pulses of electrons provide means for controlling the rates of colloidal particle growth and, hence, open the door to systematic investigations. The role of microemulsions is to compartmentalize desired amounts of Au^{3+}. Kinetic confinements within a water pool facilitate nucleation and limit the growth of gold colloids. Formation of uniform, well-separated particles is an additional advantage of preparing metal colloids in the restricted environments of surfactant aggregates.

A more precise catalyst organization was accomplished in surfactant vesicles. Cosonication of dipalmitoylphosphatidylcholine (DPPC), $[H_2C{=}CHC_6H_4NHCO(CH_2)_{10}](C_{16}H_{33})N^+(CH_3)_2,Br^-$, and K_2PtCl_4 led to the formation of spherical bilayer vesicles that contained K_2PtCl_4 in their interiors.[83] Vesicle-entrapped ions were separated from those in the bulk and/or attached to the outer surface by gel filtration and passage through an anion-exchange resin. Irradiation of Ar-bubbled, K_2PtCl_4 containing vesicles with a 450-W Xenon lamp at room temperature for 30 min resulted in the formation of colloidal platinum and the concomitant polymerization of styrene in the matrices of the vesicles. Colloid formation and polymerization

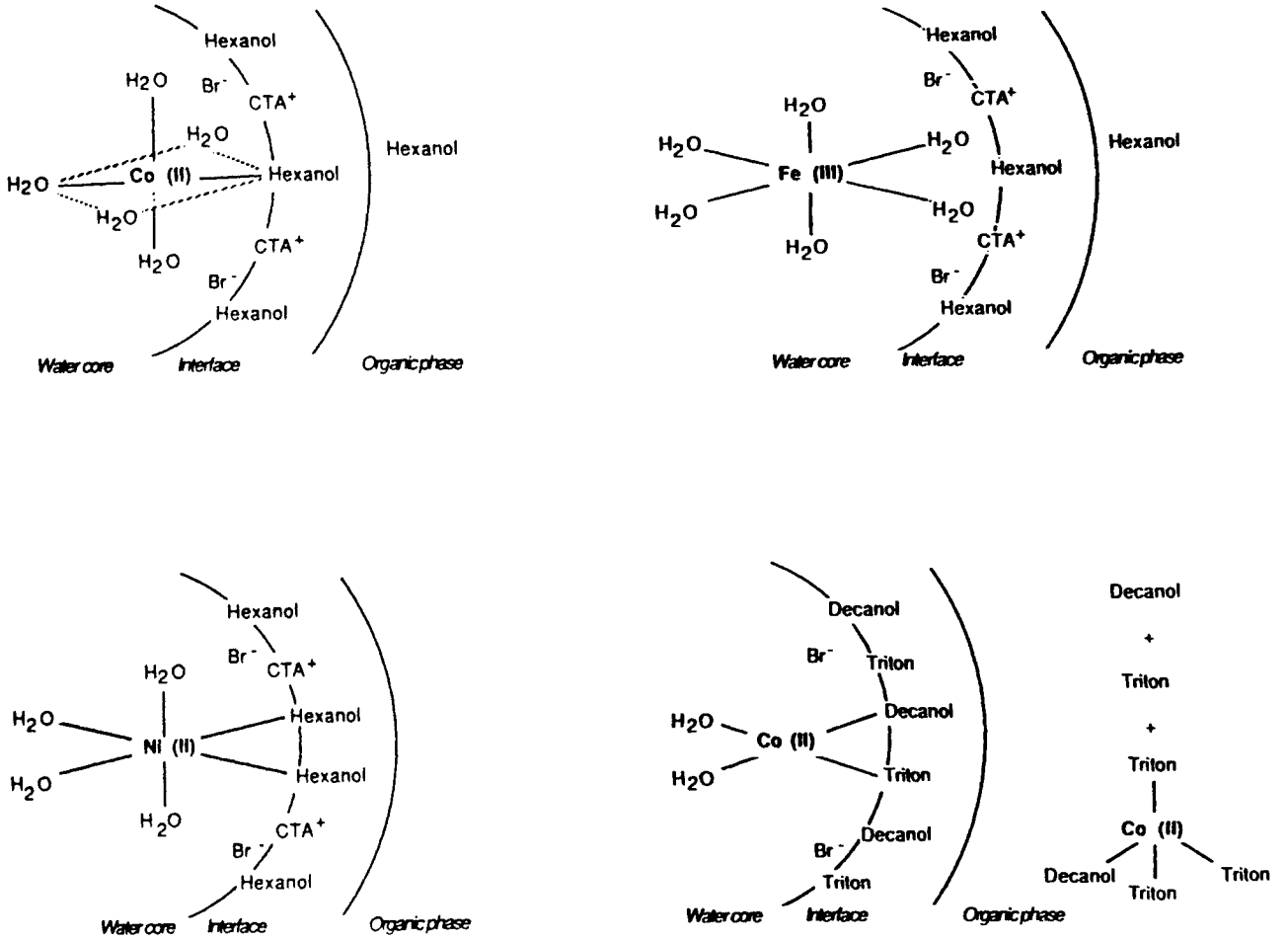

Figure 10. Models of solubilization of Ni(II), Co(II), and Fe(III) ions in the inner water cores of microemulsions. Reproduced with permission from ref 71 (copyright 1986, Plenum Press).

were monitored spectrophotometrically. Importantly, no appreciable K_2PtCl_4 could be entrapped in vesicles prepared exclusively from DPPC. Furthermore, DPPC vesicles underwent time-dependent spontaneous fusion, which, ultimately, led to their precipitation.

Colloidal platinum could also be prepared in water by irradiating 4.7×10^{-4} M K_2PtCl_4 solutions with the 450-W xenon lamp for 30 min.[83] Platinum particles were much less separated in homogeneous solutions (mean diameter 270 Å) than those entrapped in the vesicles. Furthermore, aqueous colloidal platinum, in the absence of stabilizers, precipitated within 2–3 days. Conversely, vesicle-entrapped colloidal platinum showed extraordinary stabilities: it remained stable longer than 30 days.

The catalytic efficiency of vesicle-entrapped colloidal platinum was demonstrated by the reduction of methylene blue (MB) and 10-methyl-5-deazaisoalloxazine-3-propanesulfonic acid (MAPS).[83] Bubbling of hydrogen through a solution that contained polymerized, vesicle-entrapped colloidal platinum resulted in the prompt reduction of MB or MAPS located in the vesicle bilayers (Figure 11). No reduction of MB and MAPS occurred in the absence of colloidal platinum either in vesicles or in homogeneous solutions. Externally added $FeCl_3$ could also be reduced, albeit at a very much slower rate, if hydrogen gas was bubbled through the vesicle-entrapped colloidal platinum in the absence of added MB. Apparently, $FeCl_3$ slowly penetrates even the partially polymerized vesicles.

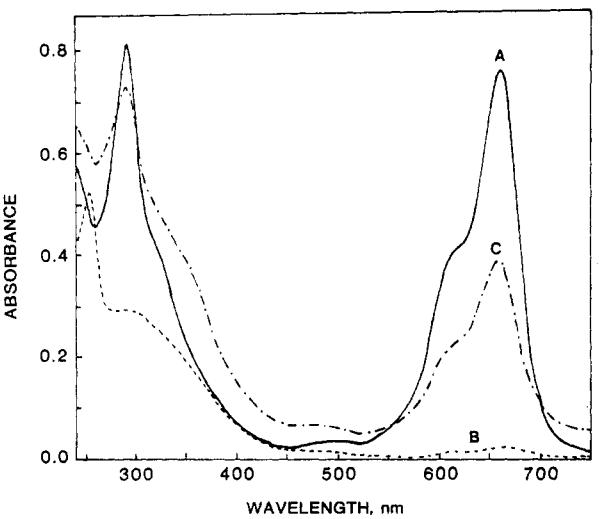

Figure 11. Absorption spectra of vesicle-entrapped colloidal platinum containing 1.07×10^{-5} M MB in its bilayers prior to hydrogen bubbling (A), subsequent to 3-min hydrogen bubbling (B), and followed by an addition of $FeCl_3$ to give an overall stoichiometric iron concentration of 2×10^{-4} M (C). The blank contained polymerized vesicles of the same concentration, and it had been bubbled by hydrogen for the same time as the sample. Reproduced from ref 83 (copyright 1983, American Chemical Society).

Reduced, polymerized, vesicle-entrapped MB or MAPS could be reoxidized by the addition of $FeCl_3$ (A in Figure 11). The process could be recycled. Bubbling of hydrogen for a few minutes caused the reduction of

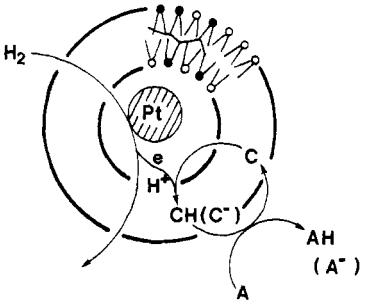

Figure 12. Use of polymerized, vesicle-entrapped colloidal platinum in catalysis. Electron and/or hydrogen carriers distributed in vesicle bilayers mediate the colloidal platinum-catalyzed reduction of extravesicular molecules by hydrogen bubbling. C and CH (or C^-) are the oxidized and reduced forms of the electron and/or hydrogen carrier, A and AH (or A^-) are the oxidized and reduced electron and/or hydrogen acceptor, and Pt is the polymerized, vesicle-entrapped, colloidal platinum catalyst. Reproduced from ref 83 (copyright 1983, American Chemical Society).

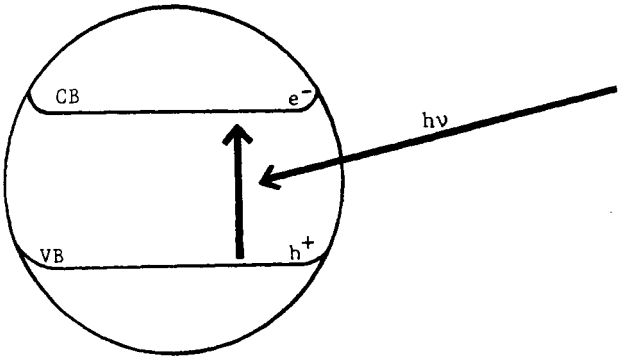

Figure 13. Schematic illustration of a colloidal semiconductor. Band-gap excitation promotes electrons from the valence band (VB) to the conduction band (CB). In the absence of electron donors and/or acceptors of appropriate potential at the semiconductor surface or close to it, most of the charge-separated, conduction-band electrons (e^-_{CB}) and valence-band holes (h^+_{VB}) nonproductively recombine. Notice the band bending at the semiconductor interface.

reoxidized MB, entrapped in the bilayers of polymerized, colloidal platinum containing vesicles. Stopping the hydrogen bubbling and addition of more $FeCl_3$ reoxidized MB. The reduction and oxidation cycles could be repeated several times (Figure 12). These observations demonstrate the feasibility of using polymeric surfactant vesicle stabilized, colloidal catalysts for reducing extravesicular molecules by hydrogen bubbling via appropriate electron and/or hydrogen carriers.

Catalytic platinum clusters generated in surfactant vesicles have also been demonstrated to catalyze hydrogenations both in situ and subsequent to their deposition on a metal grid.[84]

Well-constructed, stable Langmuir–Blodgett (LB) films offer an entry into solid-state molecular electronic devices.[89,90] The very recently reported insertion of silver ions into the hydrophilic channels of LB films and their subsequent reduction to ultrasmall (<20-Å-diameter) silver clusters illustrate the potential of this approach.[87,88] Importantly, X-ray diffraction indicated that the structure of the behemic acid matrix did not change upon the insertion of silver clusters. Sizes of the clusters were of the same dimension as the thickness of a monolayer. The rigidity of the LB matrix contributes to the stabilization of silver clusters.

IX. Semiconductors in Mimetic Membranes

Up to fairly recently, preparations, and utilizations of semiconductors have been restricted to solid-state, crystalline, microcrystalline, and amorphous systems. The entry of photophysical chemists has been signaled by their studies in dispersed colloidal semiconductors.[13,14] Their interest has primarily centered on semiconductor-mediated oxidations and reductions, particularly those related to water splitting.[9-14,91] Dispersed colloidal semiconductors offer a number of advantages. They have broad absorption spectra and high extinction coefficients at appropriate band energies. They are relatively inexpensive and can be sensitized by doping or by physical or chemical modifications. Dispersed colloidal semiconductors have high surface areas and can, therefore, function as efficient light harvesters. Subsequent to photoexcitation, colloidal semiconductors function as pools of electrons and holes (Figure 13) that, in principle, allow for multielectron-transfer processes. Colloidal semiconductors can be prepared small enough to minimize interference due to scattered light and allow direct flash photolytic investigations of electron transfers.

Unfortunately, colloidal semiconductors also suffer from a number of disadvantages. Until recently, they could not be reproducibly prepared as small (less than 20 nm in diameter), monodispersed particles. Small and uniform particles are needed to diminish nonproductive electron–hole recombinations. The smaller the semiconductor particle, the greater the chance of the escape of the charge carriers to the semiconductor surface where electron transfer can occur. There is a minimum size, however, that semiconductors must reach before absorption occurs at the bulk band gap (i.e., before the polymolecular particle becomes a semiconductor). The onset of semiconducting properties for CdS has been estimated to occur for particles whose diameters reach 6 nm. Semiconductors are difficult to maintain in solution for extended times in the absence of stabilizers. Stabilizers are bound to affect, of course, the photoelectrical behavior of semiconductors. Their modification and their coating by catalysts are, at present, more of an art than a science. Furthermore, the lifetime of electron–hole pairs in semiconductors is orders of magnitude shorter than the excited-state lifetime of typical organic sensitizers. This is due to the very much faster undesirable electron–hole recombinations than those observed in homogeneous solutions. Quantum yields for charge separations in colloidal semiconductors are, therefore, disappointingly low.

Some of these difficulties have been overcome by incorporating colloidal semiconductors into polyurethane films,[92] Nafion membranes,[93-95] and porous Vycor glass[96] and clays.[97,98] Emphasis will be placed in the present review on the use of organized surfactant aggregates as media for the in situ generation, size control, and stabilization of dispersed colloidal semiconductors. The available information is collected in Table IV.[99-114]

Available information on surface effects on CdS[115-118] has prompted the selection of this semiconductor for studies in organized surfactant assemblies. Thus, colloidal CdS was generated in situ in reversed micelles formed by sodium bis(2-ethylhexyl)sulfosuccinate (AOT).[99] Aqueous $CdCl_2$ or $Cd(NO_3)_2$ was added to

TABLE IV. Semiconductors in Mimetic Membranes

membrane mimetic system	incorporated semiconductor(s)	results	ref
AOT–isooctane–H_2O reversed micelle	50-Å-diameter CdS particles generated in situ in reversed micelles from $CdCl_2$ or $Cd(NO_3)_2$ by H_2S	reversed micelle entrapped CdS fluorescence quenched by methylviologen; band-gap excitation in the presence of Rh as catalyst and PhSH as sacrificial electron donor resulted in water photoreduction	99
AOT–heptane–H_2O reversed micelles	small (10-Å-diameter) CdS particles prepared in situ in reversed micelles from $Cd(ClO_4)_2$ and Na_2S	agglomeration number grows discontinuously; CdS fluorescence quenched by MV^{2+}	100
AOT–isooctane–H_2O reversed micelles	monodispersed CdS particles generated in situ in reversed micelles	size of CdS depended on ratio of Cd^{2+} to S^{2-}; strong fluorescence observed in the presence of excess Cd^{2+}; high yield of CdS mediated MV^{2+} photoreduction	101
Triton X-100–hexanol–cyclohexane–water reversed micelles	polydispersed CdS particles generated in situ in reversed micelles		101
AOT–isooctane–gelatin–water gels	50-Å-diameter CdS particles generated in situ	high yields of CdS mediated MV^{2+} and $Fe(CN)_6^{4-}$ photoreduction	101
AOT–isooctane–H_2O reversed micelle	TiO_2 particles prepared by mixing anhydrous isooctane solutions of titanium tetraisopropoxide with AOT–isooctane reversed micelles	$[H_2O]$ to [AOT] determines TiO_2 formation	102 103
single-compartment, 800–1000-Å-diameter dihexadecylphosphate (DHP) surfactant vesicles	CdS particles prepared in vesicles in situ from Cd^{2+} by controlled exposure to H_2S	CdS particle sizes controlled by amount of Cd^{2+} and H_2S added	104
single-compartment dioctadecyldimethylammonium chloride (DODAC) vesicles	CdS particles generated in situ in DODAC vesicles by several methods	quantum size effects for vesicle-incorporated CdS rationalized	105
single-compartment DHP vesicles	CdS particles prepared in vesicles in situ from Cd^{2+} and H_2S at inner, at outer, and at both of these surfaces	visible-light irradiation of DHP vesicle incorporated, Rh-coated CdS in the presence of PhSH as sacrificial electron donor resulted in water photoreduction	106 107
single-compartment vesicles prepared from DHP, DODAC, and $[CH_2{=}CHC_6H_4NHCO(CH_2)_{10}]$-$(C_{16}H_{33})N^+(CH_3)_2,Br^-$	CdS particles prepared in vesicles in situ from Cd^{2+} and H_2S at inner, at outer, and at both of these surfaces	sacrificial water photoreduction optimized	108
single-compartment vesicles prepared from mixtures of DODAC and $(n\text{-}C_{18}H_{37})_2N^+(CH_3)CH_2CH_2SH,Br^-$	CdS particles prepared at both the outer and inner surfaces of vesicles in situ from Cd^{2+} and H_2S	visible-light irradiation of mixed vesicle incorporated, Rh-coated CdS resulted in sacrificial water photoreduction; thiolfunctionalized surfactant acted as the sacrificial electron donor; system could be recycled	109
single-compartment DODAC vesicles	CdS particles parepared in situ in vesicles from Cd^{2+} and H_2S	sacrificial water photoreduction optimized	110
single-compartment DHP vesicles	CdS particles parpared in situ in vesicles from Cd^{2+} and H_2S	conduction band electron transfer to Rh and methylviologen examined	111
single-compartment DHP vesicles	mixed CdS–ZnS particles prepared in situ in vesicles from mixtures of Cd^{2+} and Zn^{2+} by H_2S	mixed crystals (solid solutions) or ZnS-coated CdS can be produced depending on the method of preparation	112
bilayer lipid membranes (BLMs) prepared from glycerol monooleate, phosphatidylserine, and $[n\text{-}C_{15}H_{31}CO_2(CH_2)_2]_2N^+(CH_3)$-$CH_2C_6H_4CH{=}CH_2,Cl^-$	CdS particles generated in situ on BLM surface or incorporated from the bathing solution	CdS formation monitored by simultaneous electrical and spectroscopic techniques; photovoltage, photocurrent, and semiconductor-sensitized polymerization observed on and across BLMs	113 114
bilayer lipid membranes (BLMs) prepared from glycerol monooleate, phosphatidylserine, and $[n\text{-}C_{15}H_{31}CO_2(CH_2)_2]_2N^+(CH_3)$-$CH_2C_6H_4CH{=}CH_2,Cl^-$	ZnS, PbS, CdS, CuS, Cu_2S, HgS, and In_2S_3 generated in situ on BLM surface or incorporated from the bathing solution	semiconductor formation monitored by simultaneous electrical and spectroscopic techniques	119

isooctane solutions of the surfactant to obtain a water to AOT ratio of 20. Exposure to controlled amounts of gaseous H_2S resulted in CdS formation. Excess H_2S was removed by argon bubbling. The onset of absorption of this optically clear CdS colloidal dispersion was approximately 500 nm, which is slightly blue-shifted as compared with the band gap of 520 nm (2.40 eV) of bulk crystalline CdS. Such shifts in band gap have been shown to occur in CdS particles smaller than 100 Å in diameter (Figure 5). Dynamic light-scattering measurement prior and subsequent to H_2S exposure revealed only a slight increase in the apparent radius of the water pool from 60 to 75 Å.

Reversed micelle entrapped, colloidal CdS showed the characteristic weak fluorescence emission, previously observed in homogeneous solutions.[120-123] However, the maximum emission intensity corresponded to full band-gap emission approximately 500 nm) and was not red-shifted, as observed in homogeneous solution.[121] This discrepancy might arise from the mode of preparation (H_2S instead of Na_2S) or from the specific effect of surfactant aggregates. Alternatively, this can be the result of a size distribution of the colloidal CdS particles, which could produce different band-gap energies and, hence, different fluorescence spectra. Fluorescence intensities of these solutions decayed biexponentially with lifetimes of 2.4 and 28.5 ns. Addition of 2.3×10^{-4} M methylviologen, MV^{2+}, decreased the fluorescence lifetime of the long-lived component to 18.7 ns. Similarly, addition of MV^{2+} and a surface-active viologen, $CH_2{=}C(CH_3)COO(CH_2)_{11}(C_5H_4N^+)_2CH_3,Br^-$ or $-I^-$ (RMV^{2+}), as well as PhSH, quenched the emission in-

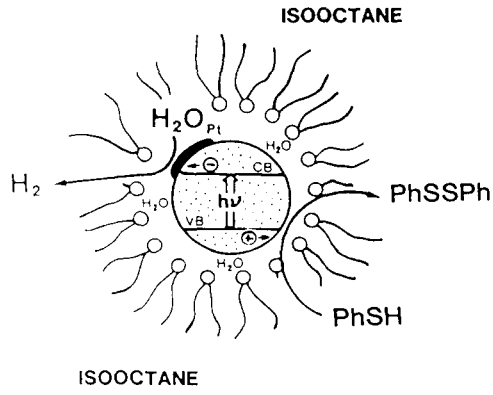

Figure 14. Idealized model for the CdS-sensitized water photoreduction by PhSH in AOT reversed micelles in isooctane. Key: VB = valence band; CB = conduction band. Reproduced from ref 99 (copyright 1984, Royal Society of Chemistry).

tensity. Apparent Stern–Volmer constants for quenching the fluorescence of colloidal CdS by MV^{2+}, RMV^{2+}, and PhSH are 2.6×10^3, 4.6×10^3, and 11.6 M^{-1}, respectively. The low quenching constant of PhSH arises from local concentration effects. Polar quenchers such as MV^{2+} and RMV^{2+} are locally concentrated in the water pool–AOT interface, whereas PhSH is homogeneously dissolved in isooctane. Due to the very fast electron–hole recombination, the quenching mechanism must be, at least in part, of static nature and dependent upon the absorbed concentration of quencher at the CdS particle surface. The Stern–Volmer appearance of the quenching data may be, therefore, coincidental.[121]

To be active in H_2 production, a catalyst has to be incorporated in the system and deposited on the semiconductor surface. Platinization was carried out by adding aqueous K_2PtCl_4 solutions to the reversed micelle entrapped, colloidal CdS and irradiating it by a 450-W xenon lamp under Ar bubbling for 30 min. Platinization was monitored spectrophotometrically.

Irradiation of degassed, reversed micelle entrapped, platinized CdS by visible lights (450-W xenon lamp, λ <350 nm) in the presence of PhSH resulted in sustained hydrogen formation. This was the consequence of electron transfer from PhSH to the positive holes in the colloidal CdS, which diminished electron–hole recombinations (Figure 14).

The reversed micelles have the specific advantage of providing a means for charge separation by continuously removing the product (PhSSPh) from the semiconductor, located in the water pool, to the organic solvent. However, due to water pool exchanges, the semiconductor particles could interact with each other, which limited the concentration of semiconductors tolerable by the system.

Surfactant vesicles offer a greater organization ability and are expected to provide greater stability for colloidal semiconductors than reversed micelles. The use of vesicles has also allowed the examination of quantum size effects.[104,105] Colloidal semiconductors can be localized at the outer, the inner, or both surfaces of single bilayer vesicles (Figure 15). Each of these arrangements has certain advantages. Semiconductors on outer vesicle surfaces are more accessible to reagents and can, therefore, more rapidly undergo photosensitized electron transfer. Smaller and more monodispersed CdS particles can be prepared and maintained

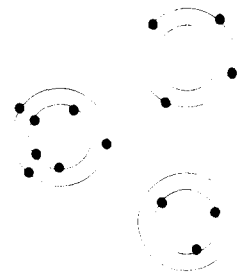

Figure 15. Schematics of available sites for organizing colloidal semiconductors in single-bilayer surfactant vesicles.

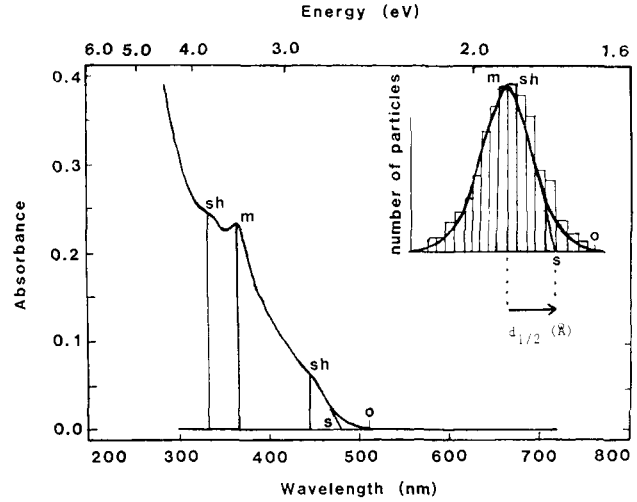

Figure 16. Absorption spectrum of CdS particles, generated in situ at the outer and inner surfaces of DODAC vesicles (preparation A). Key: sh = shoulder, m = maximum, s = absorption edge, o = onset of absorption. As shown in the insert, each $d_{1/2}$ value was obtained by taking the difference (Å) (read from a size vs. absorption maximum absorption edge calibration curve from Figure 5) between m and s. Reproduced from ref 105 (copyright 1987, American Chemical Society).

for longer times in the interior of vesicles than at any other arrangements.

Sizes of semiconductors in vesicles can be controlled by adjusting the number of precursors (Cd^{2+} ions, for example) per vesicle and/or by regulating the amount and rate of addition of H_2S. Vesicles are also efficient in maintaining colloidal particles over extended periods of time (for several months). Spatial confinements in the bilayers preclude particle growth by either agglomeration or Ostwald ripening. Different populations of semiconductors were shown to be generated at the inner and at the outer surface of DHP vesicles.[104]

More precise control of CdS particle sizes was obtained in DODAC vesicles.[98] Four different methods of preparation were investigated. In preparation A, CdS particles were generated from $CdEDTA^{2-}$ distributed at both the inner and outer surfaces of DODAC vesicles. CdS particles were localized only in the inner, or at the outer, surface of DODAC vesicles in preparations B and C, respectively. Preparation D involved the generation of CdS from Cd^{2+} ions electrostatically repulsed from the DODAC vesicle surfaces.

CdS particles were formed in preparations A–D by the careful addition of controlled amounts of H_2S. Particle sizes and size distributions have been assessed from their absorption spectra. The parameters used are defined in Figure 16. Thus, the onset of absorption (o) is defined as the wavelength at which the absorption

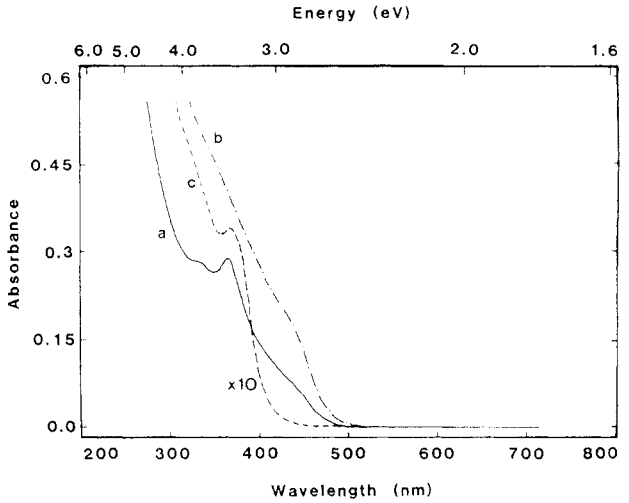

Figure 17. CdS absorption spectra formed on outer and inner (a), outer (b), and inner surface (c) alone: [DODAC] = 2.0×10^{-3} M in all systems; [$CdEDTA^{2-}$] = 2.0×10^{-4} M (a), 1.0×10^{-4} M (b) and (c); pH 9.5 (a) and (b), 10.0 (c); the spectrum of (c) is enlarged 10 times. Reproduced from ref 105 (copyright 1987, American Chemical Society).

becomes zero. The absorption edge (s) in the intersection of the base line with the tangent drawn to the absorption maximum (m, or in the case of two maxima, m_1 and m_2) or to the shoulder (sh). In the case of a pronounced maximum, the half-width of the band at the base line ($d_{1/2}$) is also determined. It should be emphasized that the obtained $d_{1/2}$ values do not correspond to sizes. They provide, however, an assessment of size distribution. The smaller the $d_{1/2}$ value, the more monodispersed are the colloid particles. Figure 17 shows the comparison of CdS spectra of particles generated on inner, outer, and both sides of DODAC vesicles.

Strictly speaking, absorption edges can only be associated with band gaps in macrocrystalline semiconductors. For particles in the 20–30-Å-diameter range, the first and second excited states generally lie at energies greater than the range at which their absorption were taken.[120] Furthermore, sizes of dispersed colloidal semiconductors vary, and their dispersity depends on the method of preparation.

Distributions of CdS particles formed in the different systems are summarized in Figure 18. In the absence of vesicles, addition of H_2S to Cd^{2+} led to broad distribution of relatively large semiconductor particles. Structureless spectra and the presence of shoulders indicated the presence of macrocrystalline particles. As seen, the smallest particles are produced in the presence of electrolytes.

Surfactant vesicles have been shown to have a myriad of advantages in the generation and stabilization of semiconductors.[104,112] They provide sites for CdS formation and shift the equilibrium between nucleation and particle growth in favor of the former. Positively charged ammonium head groups on DODAC attract $CdEDTA^{2-}$, SH^-, Cl^-, and OH^- in sufficient amounts to assume partial covering of CdS particles prior and subsequent to their incorporation into the potential field of DODAC vesicles. These anionic coatings contribute also to the stabilization of the semiconductor. The sites occupied by $CdEDTA^{2-}$ are then taken up by SH^-, which, in turn, partially surrounds, and hence

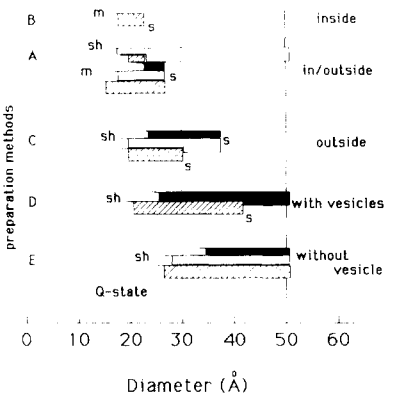

Figure 18. Sizes and size distribution of CdS particles prepared in the different systems. Bars indicate size ranges from the absorption maximum (m) or shoulder (sh) to the absorption edge (s). Open bars on the right-hand side imply absorption edges beyond 50 Å (the limit of validity on the calibration curve, see Figure 5). The "Q-state" range lies below 30-Å particle diameter. Reproduced from ref 105 (copyright 1987, American Chemical Society).

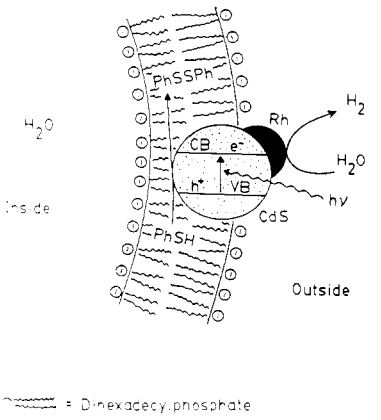

Figure 19. Idealized model for CdS-sensitized water photoreduction by PhSH in aqueous DHP vesicles. The position of the colloid in the vesicle (represented here as generated on the outside surface) is based on fluorescence quenching experiments. Reproduced from ref 103.

decreases, the lateral mobility of CdS particles, therefore stopping their further growth.

Preordaining the number of precursor molecules (Cd ions) *per* vesicle provides an important control in semiconductor formation. The concentration of DODAC *vesicles* has been calculated to be 1.2×10^{-8} M. Taking 1300 Å to be the diameter of a vesicle at 2.0×10^{-3} M, stoichiometric DODAC concentration gives 160 000 surfactant molecules/vesicle. At a concentration of 2.0×10^{-4} M $CdEDTA^{2-}$, 16 000 molecules will be attached to each DODAC vesicle, giving a ratio of DODAC to $CdEDTA^{2-}$ of 10:1.

Due to the curvature of the vesicles, there are fewer $CdEDTA^{2-}$ at the inner than at the outer surface. Consequently, there will be fewer CdS particles in the interior than at the exterior of vesicles. Also, the apparent ratio of SH^- to $CdEDTA^{2-}$ is appreciably higher in the interior of the vesicles than at their exterior or in the bulk solution. These SH^- ions will coat the CdS to such an extent as to diminish their mobility in the vesicle interior. Stability determinations are in accord with this interpretation. CdS particles in vesicle interiors remained stable appreciably longer than in the vesicle exterior.[105]

TABLE V. Quantum Yield of Hydrogen Formation at 400 nm,[a] Hydrogen Production Rates, and CdS Band Gaps in Different Vesicular Systems at 40 °C

medium[b]	CdS band gap[c]	rates of H_2 production, μmol/h: full spectrum (λ >350 nm)	mono-chromatic (400 nm)	φ (400 nm), %
HMP/water	487/100	5	1.3	0.5
DHP vesicles	490/63.3	5	1.4	1.2
DODAC vesicles	488/93.1	164	18.1	10.0
unpolymerized vesicles	463/67.1	120	9.9	7.3
polymerized vesicles	498/58.8	205	12.4	10.1

[a] $\phi = {}^1/_2$ H_2 molecule produced/photon absorbed. [b] Surfactant concentration 2×10^{-3} M, CdS 2×10^{-4} M, Rh 4×10^{-5} M, benzyl alcohol 1%, 25-mL sample, 16.1-mL gas phase. See Table IV for structural details. [c] CdS band gap (nm)/fractions of 400-nm light absorbed (%) vs. light absorbed and scattered (determined from the absorbance spectrum).

Hydrogen-generation activity of vesicle-stabilized, catalyst-coated, colloidal CdS was first demonstrated in DHP vesicles, with Rh as catalyst and thiophenol (PhSH) as sacrificial electron donor.[106,107] Figure 19 illustrates the mechanism of this photosensitized H_2 generation. The proposed position of the CdS particle (partially buried in the vesicle bilayer) was supported by the following observations: (a) CdS particles generated from externally adsorbed Cd^{2+} ions did not precipitate, even after months; therefore, they had to remain bound to the vesicle interface. (b) CdS fluorescence was efficiently quenched by PhSH, which was located in the hydrophobic membrane; therefore, the colloidal CdS particles had direct contact with the inner part of the membrane. (c) The CdS particle retained access to the surface where it originated, since entrapped polar electron acceptors such as methylviologen (MV^{2+}), while unable to penetrate the DHP membrane, could also quench the fluorescence of inner-surface-generated CdS particles. However, this quenching decreased with time, showing a gradual penetration of the CdS toward the middle of the bilayer. (d) CdS particles at the vesicle interiors remained at the inner surface of the membrane, since externally added quencher such as MV^{2+} and Rh^{3+}, while adsorbed at the outer surface of DHP vesicles, did not quench inner-surface CdS fluorescence, even after several weeks.

Although CdS could be located selectively at the inner or outer surface of the vesicles, symmetrically organized samples were found easiest to prepare most reproducibly. No significant effect of CdS location upon the photochemical activity for H_2 generation was observed.

Positively charged vesicles prepared from DODAC, $[C_{15}H_{31}CO_2(CH_2)_2]_2N^+(CH_3)(CH_2C_6H_4CH{=}CH_2),Cl^-$, and from its polymerized counterpart were found to be better media for CdS-mediated water photoreduction than that prepared from DHP.[102]

Quantum efficiency of H_2 production in the different vesicles is summarized in Table V.

Considerable basic information is being obtained by investigating semiconductor formation and properties on bilayer lipid membranes (BLMs). Simultaneous steady-state and ultrafast, time-resolved electrical and spectroscopic measurements provide a wealth of information on BLMs stabilized by polymerization and polymer coating.[113,114,119] CdS particles were, for example, generated in situ on bovine brain phosphatidylserine (PS) membranes.[114] BLMs were made by painting freshly prepared decane solutions of PS across a 0.80-mm Teflon hole separating two compartments, which contained 0.10 M aqueous KCl buffered at pH 7.4 (Tris) at ambient temperature. Thinning of the film to a 50 ± 5 Å thick BLM was monitored by observation of the reflected light, by capacitance measurements, and by intracavity laser absorption spectroscopy (ICLAS).[124] Aqueous $CdCl_2$ was added to the left-hand side of the BLM. Subsequent to a 10–15-min incubation, H_2S gas was slowly injected into the right-hand side of the BLM. Attachment of Cd^{2+} ions onto the PS BLM surface and subsequent CdS formation were monitored by voltage-dependent capacitance measurements (Figure 20).[125] The minimum in curve a is at $V = 0 \pm 2$ mV, as expected for symmetrically charged PS membranes. Displacement of the curve upon the addition of Cd^{2+} (curve b) allowed the calculation of the charge density to be $1/(360\ Å^2)$ and the surface potential difference ($\Delta\psi$) to be 66 mV. We estimate that $[Cd^{2+}]:[PS] = 1:12$. H_2S addition decreased $\Delta\psi$ to almost zero (curve c) and resulted in the development of CdS particles (see photograph and intensity changes of the reflected light). CdS formation on the BLM is also manifested in such a lowering of the amplification in the ICLAS experiments[114] that lasing stops.

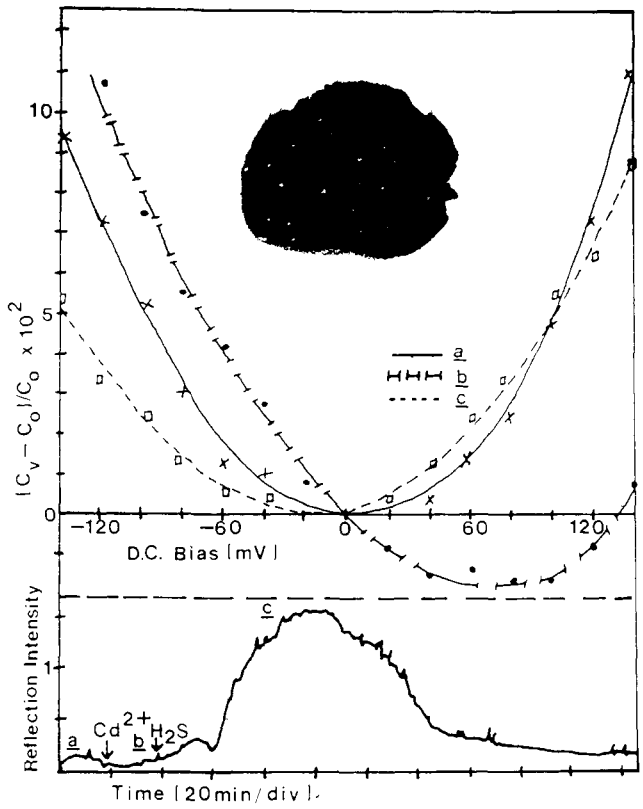

Figure 20. Upper part: Voltage-dependent capacitances of the BLMs prepared from PS prior (a) and subsequent (b) to the addition of $CdCl_2$. Curve c was obtained after H_2S addition. Grains of CdS particles are clearly seen in the photograph (inset) of the reflected light taken through a microscope. Lower part: Reflected light intensity changes on CdS formation on PS BLM. Following the addition of $CdCl_2$ (b) and H_2S, formation of CdS results in substantial increase in the intensity of the reflected light (c). Further illumination photocorrodes the CdS particles and, hence, decreases the reflected light intensity.

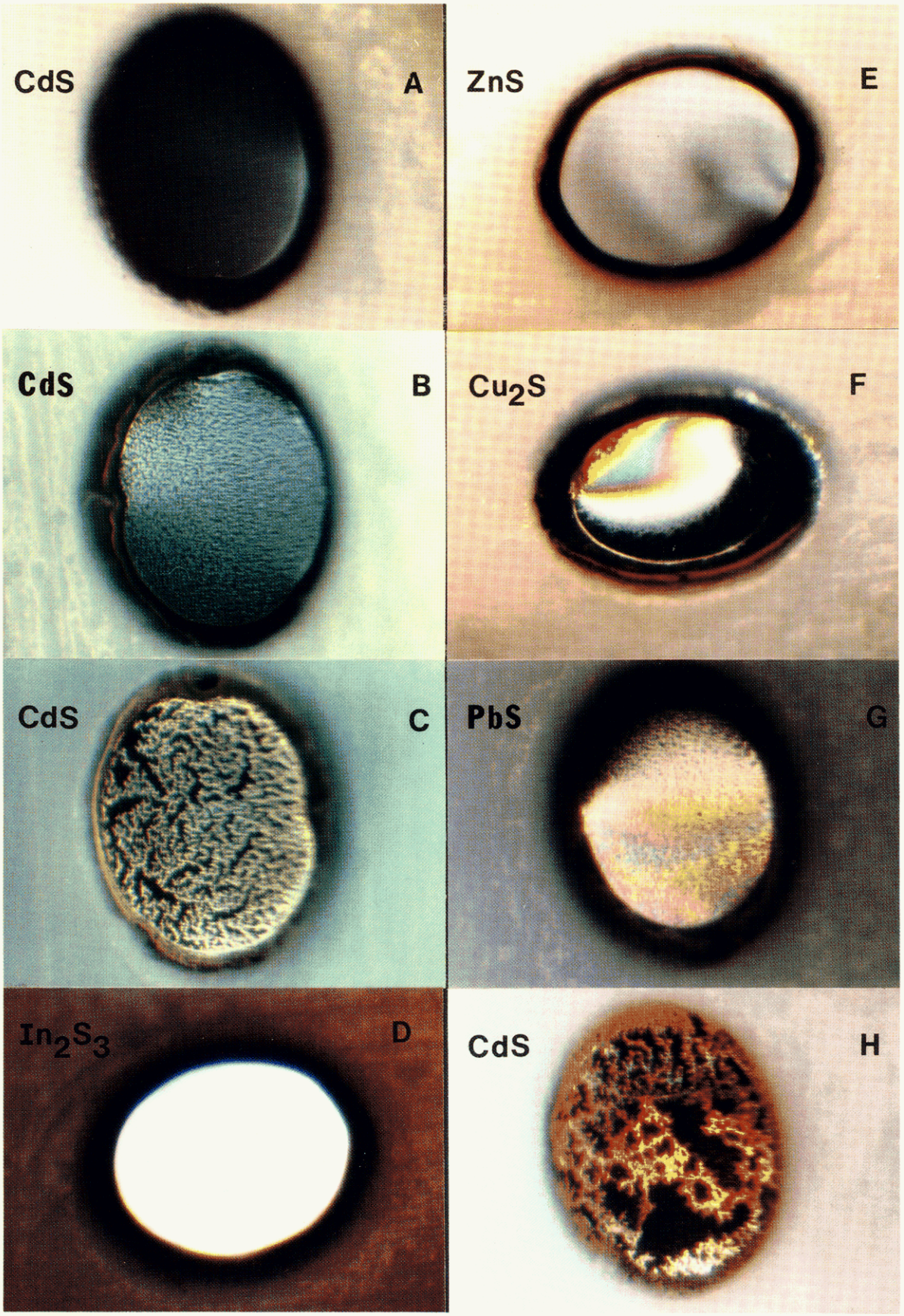

Figure 21. Micrographs of semiconductors in different stages of their growth on GMO BLMs.

CdS, ZnS, Cu_2S, In_2S_3, and PhS semiconductor clusters have also been incorporated and generated in situ on a variety of BLMs.[119] Optical microscopy of semiconductor formation on BLMs provided a wealth of morphological information. Subsequent to the injection of H_2S, the first observable change was the ap-

pearance of fairly uniform white dots of 1 μm or less on the black film (see photograph A in Figure 21). The initially formed white dots rapidly moved about the BLM surface, encountering the Plateau–Gibbs border and each other with resultant coalescence, particle growth, and island formation (see photograph B in Figure 21). The islands themselves merged, and concurrently, a second generation of white dots began to appear on the surfaces of the black channels that surrounded the enlarged white islands. The behavior of the second-generation dots was similar to that of their predecessors. They rapidly moved about, combined with each other, and ultimately coalesced into the surrounding islands (see photograph C in Figure 21). Eventually, a continuous film formed whose appearance was either that of a shiny, cloudlike layer (D) or that of a light, foglike grain layer (E). In some instances, the film formed and pressed against the Plateau–Gibbs border, and a newly developing film overlapped it. Repetition(s) of this process could lead to films of several overlapping layers, which manifested in color development (F). Color formation, albeit with less hue, could also accompany the coalescence of islands (G, H). In general, a single layer of quickly formed film was less thick than the arrested islands of particles. It needs to be emphasized that semiconductor particles, at all stages of their growth, were supported by bimolecular (black) membranes.

It is interesting to note that thin-film growth, observed electron microscopically and modeled by different theories, was discussed in terms of sequential nucleation, giving rise to islandlike structures, coalescence of the islands, channel formation, and development of the continuous film.[126]

A comparison of the color of the semiconductor deposited on the BLM with a color chart constructed for films of different thicknesses but similar refractive indices[126] allowed the assessment of the semiconductor thickness by means of eq 4, where d_s and n_s are the

$$d_s = d_o(n_o/n_s) \cos \theta_s \qquad (4)$$

thickness and refractive index of the semiconductor on the BLM, d_o and n_o are the film thickness and refractive index on the color chart corresponding to the observed color, and θ_s is the angle of refraction in the semiconductor layer, related to θ_i (angle of incident light) by Snell's Law ($n_i \sin \theta_i = n_s \sin \theta_s$). Thickness of Cu_2S (n_s = 1.5) on a GMO BLM was assessed by comparing its color with those given by the color chart for an SiO_2 (n_o = 1.46 at λ 5460 Å), using $\theta_i = 45°$ and $\theta_s = 39°$. Thus, the observed sequential color change of tan → brown → dark violet to red violet → royal blue → light to metallic blue upon the in situ generation of Cu_2S on the GMO BLM corresponded to thicknesses of 63, 88, 125, 150, and 188 nm, respectively (Figure 21F represents a later stage of Cu_2S development on the GMO BLM).[119,124]

Band-gap excitation of PS BLM incorporated CdS by a laser pulse resulted in the generation of an electron–hole pair and, in turn, in the reduction of oxygen on one side of the BLM and oxidation of HS^- on the other side, which manifested in the development of a photovoltage (Figure 22).[119] The relatively slow decay of the photovoltage is likely to be the consequence of charge recombination across the BLM. No photovoltage could be observed in the absence of CdS particles.

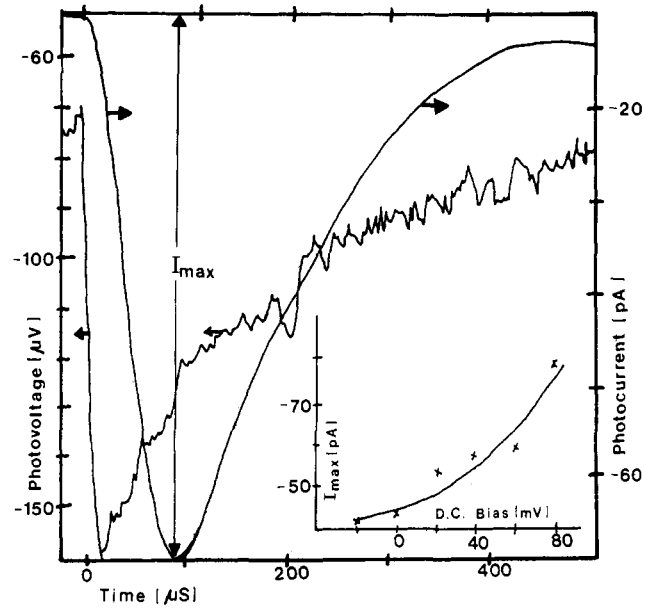

Figure 22. Excitation of CdS particles incorporated into PS BLMs by 20-ns, 1-mJ, 353-nm laser pulses results in the development of photovoltage and, in the presence of β-carotene, in the development of photocurrent. Magnitudes of the photocurrent at different DC bias voltages (+ at the CdS side of the BLM) are plotted in the inset. Reproduced from ref 119.

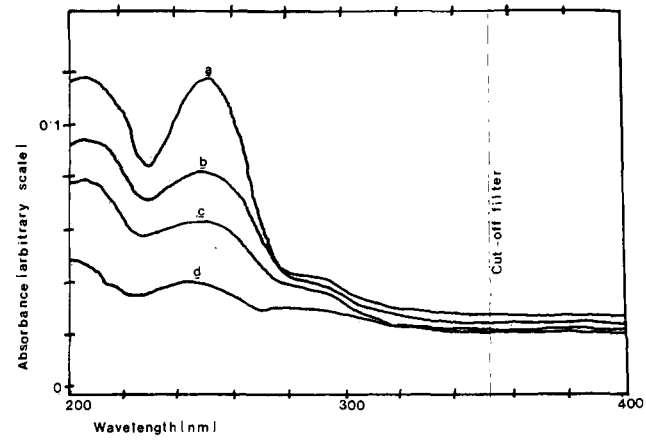

Figure 23. Band-gap excitation of CdS particles incorporated into BLMs prepared from $[n\text{-}C_{15}H_{31}CO_2(CH_2)_2]_2N^+(CH_3)(CH_2C_6H_4CH{=}CH_2),Cl^-$, by light of wavelengths longer than 350 nm for 0 (a), 2 (b), 4 (c), and 8 (d) min resulting in the polymerization of the styrene moiety of the vesicles. Reproduced from ref 114 (copyright 1987, American Chemical Society).

Laser flash excitation of CdS-containing PS BLM in the presence of 0.5% β-carotene resulted in a typical photocurrent signal (Figure 22), indicating charge transfer across the membrane. The magnitude of the charge transfer was shown to increase with increasing bias voltages (see insert in Figure 22). No photocurrent could be detected in the absence of β-carotene.[119]

Steady-state irradiation of CdS incorporated into a BLM prepared from a polymerizable surfactant, $[n\text{-}C_{15}H_{31}CO_2(CH_2)_2]_2N^+(CH_3)(CH_2C_6H_4CH{=}CH_2),Cl^-$, at wavelengths longer than 350 nm led to the loss of absorbances due to the styrene moiety (Figure 23). No absorbance losses were observed if the same BLM was irradiated at the same wavelength in the absence of CdS. Semiconductor-mediated BLM polymerization is initiated by the styrene cation radical formed by the transfer of charge to the photogenerated holes. Conduction-band electrons are likely to be scavenged by

TABLE VI. Magnetic Particles in Mimetic Membranes

membrane mimetic system	incorporated particle(s)	results	ref
AOT–isooctane (or cyclohexane)–H_2O and hexaoxyethylene–isooctane (or cyclohexane)–H_2O reversed micelles	magnetite particles prepared in situ in reversed micelles from $FeCl_2/FeCl_3$ and NH_3	coagulation of reversed micelle contained magnetite by acetone washing and drying led to magnetite particles characterized by X-ray diffraction and Mössbauer spectroscopy	130
nematic liquid crystals prepared from 35.9% sodium dodecyl sulfate, 7.2% decanol, and 56.9% water (H_2O or D_2O)	ferrofluid (1%) dispersed in the liquid crystal	stable nematic II liquid crystalline ferrofluid produced; diameter 154 ± 9.4 Å; 1.9×10^4 number of grains/cm^3; 2.20 g/cm^3 magnetization at saturation	131, 132
single-bilayer phosphatidylcholine surfactant vesicles	magnetite prepared from equimolar Fe^{2+}/Fe^{3+} and NaOH and sonicated with the lipid	X-ray analysis established the presence of magnetite in the vesicles	133
single-bilayer dioctadecyldimethylamminium chloride (DODAC) vesicles	sonication of surfactant-stabilized magnetite with DODAC	vesicle-incorporated magnetite influenced the outcome of benzophenone photolysis	134
single-bilayer dihexadecyl phosphate (DHP) vesicles	magnetite particles prepared in situ in vesicles, from Fe^{2+}/Fe^{3+} and OH^-	particles characterized by magnetic birefringence	135
single-bilayer phosphatidylcholine vesicles	magnetic particles prepared in situ from Fe^{2+}/Fe^{3+} by OH^-	particles charcterized by transmission electron microscopy, electron diffraction, and X-ray microanalysis; morphologies of intravesicular particles (spherical or disk shaped) differ from those precipitated in bulk (acircular)	67
single-bilayer DODAC vesicles	magnetite particles prepared in situ in vesicles from Fe^{2+}/Fe^{3+} and OH^-	static and dynamic polarized and depolarized light scattering, static and time-resolved dichroic anisotropy, as well as conventional magnetization vs. applied magnetic field determinations used for characterizations	136
glycerol monooleate BLM	fusion of magnetite-containing DHP vesicles to BLMS	electrical measurements and reflection spectroscopy used for characterizations	119
manganese stearate LB films	successive layers of manganese and cadmium stearates are deposited on solid support	magnetic ordering observed at $T \leq 2$ K	137
manganese stearate LB film	successive layers of manganese stearates are deposited on solid support	magnetization measured by a SQUID magnetometer in conjunction with a ^{3}He cryostat	138

oxygen. Similar CdS-sensitized polymerization of surfactant vesicles has been observed.[127]

X. Magnetic Particles in Mimetic Membranes

Compartmentalization of magnetic particles in mimetic membranes has important theoretical implications and potential practical applications. Theory clearly predicts the possibility of magnetic ordering in three-dimensional solids and the impossibility of such ordering in one-dimensional solids.[128,129] Prediction, however, is model dependent for two-dimensional solids. Two-dimensional magnetic ordering is only compatible with the Ising model, which considers the magnetic spin interactions to be constrained in a single direction. Conversely, interaction of the magnetic spins are allowed in any direction in the Heisenberg model and in the plane in the x–y model. The tenet of the present review is that mimetic membranes provide eminently suitable systems for the experimental testing of these theories. Further, it is believed that inspiration for the construction of magnetic particles with controllable dimensions can be gained by studying biomineralization. The paucity of work in this area (see Table VI)[130–138] is truly surprising. Even ferrofluids are usually obtained by methods of brute force.[139]

Magnetic particles were also incorporated into poly(ethylene glycol)-modified lipase.[140] The activity of the lipase remained unaltered in the presence of magnetite; this allowed the magnetic separation of the reaction mixture from the enzyme—a considerable advantage for scaling up enzyme-mediated syntheses. Reversed micelles,[130] liquid crystals,[131,132] vesicles,[133–136] BLMs,[119] and LB films[137,138] have been shown to serve as media for magnetic particles.

The organizational advantage is best illustrated by the realization of magnetic effects on a chemical reaction even in the absence of an externally applied magnetic field.[134] The underlying principle of these effects is based on the chemically induced dynamic nuclear polarization model.[141–144] According to this theory, the chemical reactivity of radical pairs is expected to depend on the hyperfine interactions of the orbitally uncoupled electrons with the magnetic field. One good example is found in the photoreduction of benzophenone [$(C_6H_5)_2C{=}O$ (BP)], to diphenylcarbinol [$(C_6H_5)_2CHOH$] and to minor light-absorbing products.[132–134] Product formation has been explained in terms of the decay of the photolytically generated benzophenone triplets (^{3}BP*) in the presence of a hydrogen donor (RH) to a caged triplet radical pair, ^{3}[BṖH + Ṙ]. The triplet radical pair in turn undergoes competitive intersystem crossing to a caged singlet radical pair, ^{1}[BṖH + Ṙ], with the escape of the radicals from their cages:

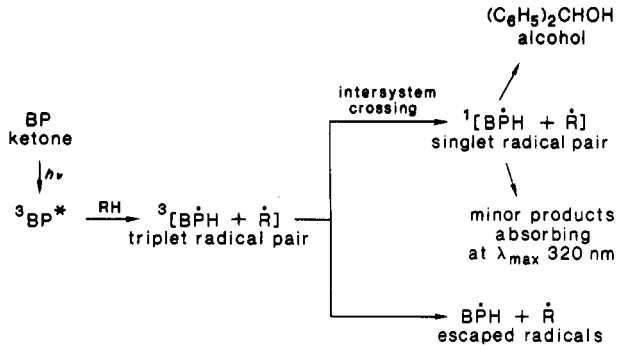

Incorporation of magnetic particles (Fe_3O_4) into vesicles prepared from DODAC has an effect on benzophenone photolysis that is identical with that for an externally applied magnetic field of 2000 G. The percentages of radicals that escape increased from 56% to 87%.[134] This dramatic alteration of benzophenone photochemistry originates in the localization of benzophenone within the influence of single-domain magnetic particles confined in the matrices of surfactant vesicles (Figure 24). Magnetic particles, which are in close proximity, effectively split the triplet sublevels of the radical pair and slow down intersystem crossing from triplet levels. This, in turn, enhances the efficiency of radical escape manifested in decreased production of light-adsorbing products. Thus, the observed effect of the photochemistry of benzophenone is a direct result of the magnetic moment in the vicinity of the magnetic particles.

Particularly significant is the observation of two-dimensional magnetism in LB films.[137] Spreading of stearic acid on a trough containing cadmium ions and their subsequent deposition led to a monomolecular layer of cadmium stearate on a solid support. Repeating twice the spreading on an aqueous solution of manganese, rather than Cd^{2+} ions, led to the deposition of two layers of manganese stearate ions (Figure 25). Magnetic ordering of the manganese ions between the hydrophilic channels of two monolayers was established by electron paramagnetic spectroscopy at 2 K. The nature of the ordering was suggested to be predominantly antiferromagnetic, with a weak ferromagnetic component.[137] Additional work is required for the full characterization of this intriguing system. We can fully expect the realization of different types of magnetisms in mimetic membranes.

XI. Conclusion

Appreciable progress has been made in utilizing mimetic membranes as hosts for microcrystals, catalysts, semiconductors, and magnetic particles. In many cases, size and morphology control and long-term stabilities have been accomplished. Advantage has often been taken of the unique microenvironments surrounding the mimetic membrane incorporated clusters to drive chemical processes. A more thoughtful analysis of the data compiled in the tables reveals the paucity of published work. Available opportunities have been barely touched. The mimetic approach to cluster formation and utilization is only in its infancy. There is a great deal to be learned from biomineralization. I am confident that the interdisciplinary nature of this area will attract a variety of researchers who will make significant breakthroughs.

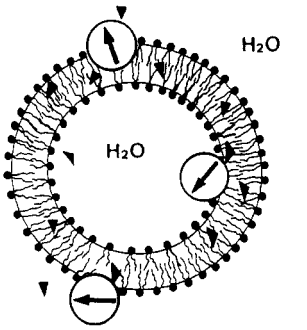

Figure 24. Artist's conception of colloidal Fe_3O_4 particles incorporated in dioctadecyldimethylammonium cation vesicles containing benzophenone (▼). Positions and dimensions of Fe_3O_4 particles need not be taken literally.

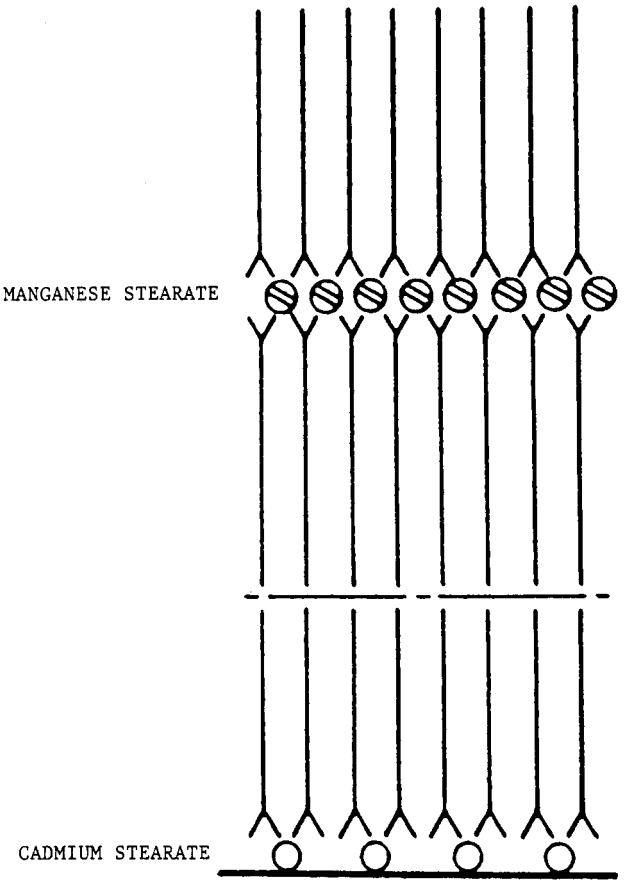

Figure 25.

XII. Acknowledgment

I thank my co-workers, whose names appear in joint original publications, for their enthusiastic, dedicated, and skillful work. The National Science Foundation, Department of Energy, and Army Research Office provided financial support for the different aspects of our researches. Helpful comments made by S. Mann, M. P. Pileni, J. K. Thomas, J. B. Nagy, P. Stenius, and S. Baral on an earlier version of this manuscript are gratefully appreciated.

XIII. References

(1) Bittar, E. E. *Membrane Structure and Function*; Wiley-Interscience: New York, 1980.
(2) Jain, M. K.; Wagner, R. C. *Introduction to Biological Membranes*; Wiley-Interscience: New York, 1980.
(3) Robertson, N. *The Lively Membranes*; Cambridge University: Cambridge, 1983.

(4) Hoppe, W.; Lohmann, W.; Markl, H.; Ziegler, H. *Biophysics*; Springer-Verlag: Berlin, 1983.
(5) Fendler, J. H. *Membrane Mimetic Chemistry*; Wiley: New York, 1982.
(6) Fendler, J. H. *Chem. Eng. News* **1984**, *62*(Jan 2), 25.
(7) Fendler, J. H. *Science (Washington, D.C.)* **1984**, *223*, 888.
(8) Fendler, J. H.; Fendler, E. J. *Catalysis in Micellar and Macromolecular Catalysis*; Academic: New York, 1975.
(9) Calvin, M. *Acc. Chem. Res.* **1978**, *11*, 369.
(10) Porter, G. *Proc. R. Soc. London, A* **1978**, *362*, 281.
(11) Grätzel, M. *Acc. Chem. Res.* **1981**, *14*, 376.
(12) Fendler, J. H. *J. Phys. Chem.* **1980**, *84*, 1485.
(13) Fendler, J. H. *J. Phys. Chem.* **1985**, *89*, 2730.
(14) Thomas, J. K. *J. Phys. Chem.* **1987**, *91*, 267.
(15) Wennerstrom, H.; Lindman, B. *Phys. Rev.* **1979**, *52*, 1.
(16) Fendler, J. H. *Acc. Chem. Res.* **1976**, *9*, 153.
(17) Eicke, H. F. *Top. Curr. Chem.* **1980**, *87*, 85.
(18) Luisi, P. L.; Straub, E. *Reversed Micelles*; Plenum: New York, 1984.
(19) Kertes, A. S.; Gutman, H. *Surf. Colloid Sci.* **1975**, *8*, 193.
(20) Luisi, P. L.; Magid, L. J. *CRC Crit. Rev. Biochem.* **1986**, *20*, 409.
(21) Gaines, G. L., Jr. *Insoluble Monolayers at Liquid-Gas Interfaces*; Interscience: New York, 1966.
(22) Kuhn, H.; Möbius, D. *Angew. Chem., Int. Ed. Engl.* **1971**, *10*, 620.
(23) Gun, J.; Iscovici, R.; Sagiv, J. *J. Colloid Interface Sci.* **1984**, *101*, 201.
(24) Tien, H. T. *Bilayer Lipid Membranes (BLM), Theory and Practice*; Marcel Dekker: New York, 1974.
(25) Montal, M.; Mueller, P. *Proc. Natl. Acad. Sci. U.S.A.* **1976**, *69*, 3561.
(26) White, S. H.; Petersen, D. C.; Simon, S.; Yafuso, M. *Biophys. J.* **1976**, *16*, 481.
(27) Fendler, J. H. *Acc. Chem. Res.* **1980**, *13*, 7.
(28) Fendler, J. H. In *Surfactants in Solution*; Mittal, K. L., Lindman, B., Eds.; Plenum: New York, 1984; p 1947.
(29) Fendler, J. H.; Tundo, P. *Acc. Chem. Res.* **1984**, *17*, 3.
(30) Paleos, C. M. *Chem. Soc. Rev.* **1985**, *14*, 45.
(31) Bader, H.; Dorn, K.; Hashimoto, K.; Hupfer, B.; Petropoulos, J. H.; Ringsdorf, H.; Sumimoto, H. In *Polymer Membranes*; Gordon, M., Ed.; Springer-Verlag: Berlin, 1985; p 1.
(32) Lowenstam, H. A. *Science (Washington, D.C.)* **1981**, *211*, 1126.
(33) Westbrook, P.; de Jong, E. W. *Biomineralization and Biological Metal Accumulation*; Reidel: Dordrecht, Holland, 1983.
(34) Mann, S. *Struct. Bonding (Berlin)* **1983**, *54*, 125.
(35) Weiner, S. *CRC Crit. Rev. Biochem.* **1986**, *20*, 365.
(36) Veis, A. *The Chemistry and Biology of Mineralized Connective Tissue*; Elsevier; North-Holland: Amsterdam, 1981.
(37) Mann, S. *J. Inorg. Biochem.* **1986**, *28*, 363.
(38) Williams, R. J. P. *Philos. Trans. R. Soc. Lond., B* **1974**, *304*, 411.
(39) Nancolles, G. H. *Adv. Colloid Interface Sci.* **1979**, *10*, 215.
(40) Addadi, L.; Berkovich-Yellin, Z.; Weissbuch, I.; van Mil, J.; Simon, L.; Lahav, M.; Lieserowitz, L. *Angew. Chem., Int. Ed. Engl.* **1985**, *24*, 466.
(41) Torres de Araujo, F. F.; Pires, M. A.; Frankel, R. B.; Bicudo, C. E. M. *Biophys. J.* **1986**, *50*, 375.
(42) Ofer, S.; Nowik, I.; Bauminger, E. R.; Papefthymiou, C. C.; Frankel, R. B.; Blakemore, R. P. *Biophys. J.* **1984**, *46*, 57.
(43) Ostwald, W. *Die Welt der Vernachlassigten Dimensionen*; Steinkopff: Dresden, 1920.
(44) Weller, H.; Koch, V.; Gutierrez, M.; Henglein, A. *Ber. Bunsenges. Phys. Chem.* **1984**, *88*, 649.
(45) Fojtik, A.; Weller, H.; Koch, V.; Henglein, A. *Ber. Bunsenges. Phys. Chem.* **1984**, *88*, 969.
(46) Rosetti, R.; Nakahara, S.; Brus, L. E. *J. Chem. Phys.* **1983**, *79*, 1086.
(47) Brus, L. E. *J. Chem. Phys.* **1984**, *80*, 4403. Brus, L. E. In *Dynamics on Surfaces*; Pullman, B., Ed.; Reidel: New York, 1984; p 431.
(48) Rosetti, R.; Ellison, J. L.; Gibson, J. M.; Brus, L. E. *J. Chem. Phys.* **1984**, *80*, 4464.
(49) Nozik, A. J.; Williams, F.; Nenadovic, M. T.; Rahj, T.; Mičič, O. I. *J. Phys. Chem.* **1985**, *89*, 397.
(50) Brus, L. *J. Phys. Chem.* **1986**, *90*, 2555.
(51) Brus, L. *J. Chem. Phys.* **1983**, *79*, 5566.
(52) Brus, L. *J. Chem. Phys.* **1984**, *80*, 4403.
(53) Fojtik, A.; Weller, H.; Koch, V.; Henglein, A. *Ber. Bunsenges. Phys. Chem.* **1984**, *88*, 969.
(54) Weller, H.; Schmidt, H. M.; Koch, V.; Fojtik, A.; Baral, S.; Henglein, A.; Kunath, W.; Weiss, K.; Dreman, E. *Chem. Phys. Lett.* **1986**, *124*, 557.
(55) Nemeljkovic, J. M.; Nenadovic, M. T.; Mičič, O. I.; Nozik, A. J. *J. Phys. Chem.* **1986**, *90*, 12.
(56) Hiemenz, P. C. *Principles of Colloid and Surface Chemistry*; Marcel Dekker: New York, 1977.
(57) Dvolaitzky, M.; Ober, K.; Taupin, C.; Anthore, R.; Auvray, X.; Petipas, C.; Williams, C. *J. Dispersion Sci. Technol.* **1983**, *4*, 29.
(58) Leung, R.; Hou, J.; Manohar, C.; Shah, D. O.; Chun, P. W. *ACS Symp. Ser.* **1985**, *No. 272*, 325.
(59) Kon-no, K.; Koide, M.; Kitahara, A. *Nippon Kagaku Kaishi* **1984**, *6*, 815.
(60) Kandori, K.; Kon-no, K.; Kitahara, A.; Fujiwara, M.; Tamura, T. Proceedings of the Sixth International Symposium on Surfactants in Solution—Modern Aspects, New Delhi, India, Aug 18–22, 1986.
(61) Palkar, U. R.; Multani, M. S.; Aygub, P. Proceedings of the Sixth International Symposium on Surfactants in Solution—Modern Aspects, New Delhi, India, Aug 18–22, 1986.
(62) Hutchinson, J. L.; Mann, S.; Skarnulis, A. J.; Skarnulis, A. J.; Williams, R. J. P. *J. Chem. Soc., Chem. Commun.* **1980**, 634.
(63) Mann, S.; Williams, R. J. P. *J. Chem. Soc., Dalton Trans.* **1983**, 311.
(64) Mann, S.; Kime, M. J.; Ratcliffe, R. G.; Williams, R. J. P. *J. Chem. Soc., Dalton Trans.* **1983**, 771.
(65) Skarnulis, A. J.; Strong, P. J.; Williams, R. J. P. *J. Chem. Soc., Chem. Commun.* **1978**, 1030.
(66) Mann, S.; Skarnulis, A. J.; Williams, R. J. P. *Isr. J. Chem.* **1981**, *21*, 3.
(67) Mann, S.; Hannington, S. P.; Williams, R. J. P. *Nature (London)* **1986**, *324*, 565.
(68) Somorjai, G. A. *Adv. Catal.* **1977**, *26*, 1.
(69) Boudart, M.; McDonald, M. A. *J. Phys. Chem.* **1984**, *88*, 2185.
(70) Lin, Z. Z.; Okuhara, T.; Misono, M.; Tohji, K.; Udagawa, Y. *J. Chem. Soc., Chem. Commun.* **1986**, 1673.
(71) B.Nagy, J.; Deroune, E. J.; Gourgue, A.; Lufimpadio, N.; Ravet, I.; Verfaillie, J. P. Proceedings of the Sixth International Symposium on Surfactants in Solution—Modern Aspects, New Delhi, India, Aug 18–22, 1986.
(72) Ozin, G. A. *CHEMTECH* **1985**, 488.
(73) Marignier, J. L.; Belloni, J.; Delcourt, M. O.; Chevalier, J. P. *Nature (London)* **1985**, *317*, 344.
(74) Matijević, E. *Acc. Chem. Res.* **1981**, *14*, 22.
(75) Boutonnet, M.; Kizling, J.; Stenius, P.; Maire, G. *Colloids Surf.* **1982**, *5*, 209.
(76) Boutonnet, M.; Kizling, J.; Touroude, R.; Maire, G.; Stenius, P. *Appl. Catal.* **1986**, *20*, 163.
(77) Boutonnet, M.; Kizling, J.; Mintsa-Eya, V.; Choplin, A.; Touroude, R.; Maire, G.; Stenius, P. *J. Catal.*, in press.
(78) B.Nagy, J.; Gourgue, A.; Derouane, E. G. In *Preparation of Catalysts, III*; Poncelet, G., Grange, P., Jacobs, P. A., Eds.; Elsevier: Amsterdam, 1983; p 193.
(79) Ravet, I.; Gourgue, A.; Gabelica, Z.; B.Nagy, J. Proceedings of the Eighth International Congress on Catalysis, West Berlin, Germany, July 2–6, 1984; Vol. IV, p 871.
(80) Lufimpadio, N.; B.Nagy, J.; Derovane, E. G. In *Surfactants in Solution*; Mittal, K. L., Lindman, B., Eds.; Plenum: New York, 1984; p 1483.
(81) Ravet, I.; Lufimpadio, N.; Gourgue, A.; B.Nagy, J. *Acta Chim. Hung.* **1985**, *119*, 155.
(82) Kurihara, K.; Kizling, J.; Stenius, P.; Fendler, J. H. *J. Am. Chem. Soc.* **1983**, *105*, 2574.
(83) Kurihara, K.; Fendler, J. H. *J. Am. Chem. Soc.* **1983**, *105*, 6152.
(84) Kurihara, K.; Fendler, J. H.; Ravet, I.; B.Nagy, J. *J. Mol. Catal.* **1986**, *34*, 325.
(85) Toshima, N.; Takahashi, T.; Hirai, H. *Chem. Lett.* **1986**, 35.
(86) Toshima, N.; Takahashi, T.; Hirai, H. *Chem. Lett.* **1985**, 1245.
(87) Leloug, J.; Maire, P.; Ruaudel-Teixier, A.; Barraud, A. *J. Chim. Phys.-Chim. Biol.* **1985**, *82*, 695.
(88) Ruaudel-Teixier, A. Leloup, J.; Barraud, A. *Mol. Cryst. Liq. Cryst.* **1986**, *134*, 347.
(89) Simon, J.; André, J. J. *Molecular Semiconductors*; Springer-Verlag: Berlin, 1985.
(90) Carter, F. *Molecular Electronic Devices*; Marcel Dekker: New York, 1982.
(91) Fox, M. A. *Acc. Chem. Res.* **1983**, *16*, 314.
(92) Meissner, D.; Memming, R.; Kastening, B. *Chem. Phys. Lett.* **1983**, *96*, 34.
(93) Krishnan, M.; White, J. R.; Fox, M. A.; Bard, A. J. *J. Am. Chem. Soc.* **1983**, *105*, 7002.
(94) Mau, A. W.-H.; Huang, C. B.; Kakuta, N.; Bard, A. J.; Campion, A.; Fox, M. A.; White, J. M.; Webber, S. E. *J. Am. Chem. Soc.* **1984**, *106*, 6537.
(95) Kuczynski, B. H.; Milosavjevic, B. H.; Thomas, J. K. *J. Phys. Chem.* **1984**, *88*, 980.
(96) Kuczynski, J.; Thomas, J. K. *J. Phys. Chem.* **1985**, *89*, 2720.
(97) Enea, O.; Bard, A. J. *J. Phys. Chem.* **1986**, *90*, 301.
(98) Stramel, R. D.; Nakamura, T.; Thomas, J. K. *Chem. Phys. Lett.* **1986**, *130*, 423.
(99) Meyer, M.; Wallberg, C.; Kurihara, K.; Fendler, J. H. *J. Chem. Soc., Chem. Commun.* **1984**, 90.
(100) Lianos, P.; Thomas, J. K. *Chem. Phys. Lett.* **1986**, *125*, 299.

(101) Pileni, M. P., unpublished results.
(102) Tricot, Y.-M.; Rafaeloff, R.; Emeren, Å.; Fendler, J. H. *ACS Symp. Ser.* **1985**, *No. 278*, 99.
(103) Meyer, M.; Kurihara, K.; Fendler, J. H., unpublished results.
(104) Tricot, Y.-M.; Fendler, J. H. *J. Phys. Chem.* **1986**, *90*, 3369.
(105) Watzke, H. J.; Fendler, J. H. *J. Phys. Chem.*, in press.
(106) Tricot, Y.-M.; Fendler, J. H. *J. Am. Chem. Soc.* **1984**, *106*, 2475.
(107) Tricot, Y.-M.; Fendler, J. H. *J. Am. Chem. Soc.* **1984**, *106*, 7359.
(108) Tricot, Y.-M.; Emeren, Å.; Fendler, J. H. *J. Phys. Chem.* **1985**, *89*, 4721.
(109) Rafaeloff, R.; Tricot, Y.-M.; Nome, F.; Tundo, P.; Fendler, J. H. *J. Phys. Chem.* **1985**, *89*, 1236.
(110) Rafaeloff, R.; Tricot, Y.-M.; Nome, F.; Fendler, J. H. *J. Phys. Chem.* **1985**, *89*, 533.
(111) Youn, H. C.; Tricot, Y.-M.; Fendler, J. H. *J. Phys. Chem.*, in press.
(112) Youn, H. C.; Baral, S.; Fendler, J. H., unpublished results.
(113) Rolandi, R.; Flom, S. R.; Dillon, I.; Fendler, J. H. *Prog. Colloid Polym. Sci.*, in press.
(114) Baral, S.; Zhao, X. K.; Rolandi, R.; Fendler, J. H. *J. Phys. Chem.*, in press.
(115) Kuczynski, J. P.; Thomas, J. K. *Chem. Phys. Lett.* **1982**, *88*, 445.
(116) Kuczynski, J. P.; Milosavljevic, B. H.; Thomas, J. K. *J. Phys. Chem.* **1983**, *87*, 3368.
(117) Kuczynski, J. P.; Thomas, J. K. *J. Phys. Chem.* **1983**, *87*, 5498.
(118) Kuczynski, J.; Thomas, J. K. *Langmuir* **1985**, *1*, 158.
(119) Zhao, X. K.; Baral, S.; Fendler, J. H., unpublished results.
(120) Henglein, A. *Ber. Bunsenges. Phys. Chem.* **1982**, *86*, 301.
(121) Ramsden, J. J.; Grätzel, M. *J. Chem. Soc., Faraday Trans. 1* **1984**, *80*, 919.
(122) Rosetti, R.; Brus, L. *J. Phys. Chem.* **1982**, *86*, 4470.
(123) Kuczynski, J. P.; Milosavljevic, B. H.; Thomas, J. K. *J. Phys. Chem.* **1983**, *87*, 3368.
(124) Zhao, X. K.; Fendler, J. H. *J. Phys. Chem.* **1986**, *90*, 3886.
(125) Alvarez, O.; Latorre, R. *Biophys. J.* **1978**, *21*, 1.
(126) Neugebauer, C. E. In *Handbook of Thin Film Technology*; Maissel, L. I., Glang, R., Eds.; McGraw-Hill: New York, 1970; Chapter 8.
(127) Fäldt, P.; Baral, S.; Fendler, J. H., unpublished results.
(128) Pomerantz, M. In *Phase Transitions in Surface Films*; Dash, J. G., Ruvalds, J., Eds.; Plenum: New York, 1980; p 317.
(129) Pomerantz, M. *Surf. Sci.* **1984**, *142*, 556.
(130) Gobe, M.; Kon-no, K.; Kandori, K.; Kitahara, A. *J. Colloid Interface Sci.* **1983**, *93*, 293.
(131) Libert, L.; Martinet, A. *J. Phys. Lett.* **1979**, *40*, L-363.
(132) Libert, L.; Martinet, A. *IEEE Trans. Magn.* **1980**, *MAG-16*, 266.
(133) Mann, S.; Skarnulis, A. J.; Williams, R. J. P. *J. Chem. Soc., Chem. Commun.* **1979**, 1067.
(134) Herve, P.; Nome, F.; Fendler, J. H. *J. Am. Chem. Soc.* **1984**, *106*, 8291.
(135) Watzke, H.; Szczurek, A.; Fendler, J. H., unpublished results.
(136) Reed, W.; Fendler, J. H. *J. Appl. Phys.* **1986**, *59*, 2914.
(137) Aviram, A.; Pomerantz, M. *Solid State Commun.* **1982**, *41*, 297.
(138) Asaolu, I. A.; Blott, B. H.; Khan, W. I.; Melville, D. *Thin Solid Films* **1983**, *99*, 263.
(139) Charles, S. W.; Popplewell, J. In *Ferromagnetic Materials*; Wohlfarth, E. P., Ed.; North-Holland: Amsterdam, 1980; Vol. 2, p 509.
(140) Takahashi, K.; Tamamura, Y.; Kodera, Y.; Mihama, T.f Saito, Y.; Inada, Y. *Biochem. Biophys. Res. Commun.* **1987**, *142*, 291.
(141) Buchachenko, A. L. *Russ. Chem. Rev. (Engl. Transl.)* **1976**, *45*, 761.
(142) Turro, N. J.; Krautler, B. *Acc. Chem. Res.* **1980**, *13*, 369.
(143) Turro, N. J. *Proc. Natl. Acad. Sci. U.S.A.* **1983**, *80*, 609.
(144) Lawler, F. *Acc. Chem. Res.* **1972**, *5*, 25.
(145) Scaiano, J. C.; Aubuin, E. B. *Chem. Phys. Lett.* **1981**, *81*, 209.
(146) Scaiano, J. C.; Lougnot, D. J. *J. Phys. Chem.* **1984**, *88*, 3379.
(147) Sakaguchi, Y.; Hayashi, H.; Nagakure, J. *J. Phys. Chem.* **1982**, *86*, 3177.